Egypt. J. Chem. **Vol. 68,** No. 10 pp. 287 - 321 (2025)

Egyptian Journal of Chemistry

http://ejchem.journals.ekb.eg/

In Vitro, In Silico Biochemical Evaluation Of Some Candidate Drugs As Anticancer. A Facile Rout for Synthesis of Novel 3-(2-Aminothiazole-4-Yl)-2H-Chromen-2-One-Based Heterocycles and Their Relation to Physical Therapy

Taha M. A Eldebss[a]*, Mohamed. K. Alboqai[b] , Abd El MonaemAEl Torgoman[c] and Shaimaa A Hassanand

[a]Department of Chemistry, Faculty of Science ,University of Cairo ,Giza121613 Egypt
[b]Bioscience Specialty of Rehabilitation, Science of Body Engineering, Irbid National University, Irbid, Jordan
[c]Department of Chemistry, Faculty of Science ,University of , Menoufia, Egypt

Abstract new series derived from 3-(2-aminothiazole-4-yl)-2H-chromen-2-one was synthesized, characterized and its pharmacological activity toward epidermal growth factor receptor (EGFR) inhibition was screened as a part of our ongoing search for new bioactive molecules. The newly synthesized compounds were confirmed by elemental analysis, IR, 1H NMR, 13 C- NMR and mass spectral data. A total 5 new synthesized compounds were evaluated for their in-vitro anticancer activities and their potential tumor cell growth inhibitory activity against human liver cancer cell line (HEPG-2) and human breast cancer cell line (MCF-7) and human colon cancer cell line (HCT-116). The results obtained indicated that some of such compounds showed promising anticancer activities.The most active compound of the series was 9, showing IC50 value of 4.1 µg compared to doxorubcin with IC50 of 2.1 µg and vinblatine with IC50 of 4.6 µg.
Also the best computational method with exchange–correlation energy functional DFT/B3LYP/6-311++G (d,p) level of theory decided to compute molecular properties of the hybrid Coumarin derivatives (2,3-4a,4b,8 and 9). We determined the molecular electrostatic surface potential (MESP) to determine the most active site in these derivatives series with high quality informative and visualization. We have applied structure activity/property relationship for all proposed derivatives indicate that the proposed compounds exhibit good oral bioavailability and also Coumarin derivative (9) have a good biological activity which needs a drug delivery carrier to deposit on the surface of suitable nanomaterial with specific properties to enhance oral bioavailability which is very near to optimal value range. molecular docking and molecular dynamics simulation (MDS) techniques runs for 100 ns for the best docked complexes (1M17-4b and 1M17-9). Free binding energies technique MM/GBSA and PBSA are performed using snapshots taken from the systems trajectories 100 ns. These results revealed that the 1M17-9complex system acquired a relatively more stable conformation and even better descriptors than the other 1M17-4bcomplex studied systems, which indicates that it is highly amenable to inhibition Epidermal Growth Factor Receptor tyrosine kinase domain (TKD) which is excellent correlation with experimentally biological effectiveness of the designed drug construct.

Keywords: EGFR inhibitors, IC_{50}, erltornib, molecular docking studies, coumarin.

1. Introduction

A broad spectrum of activity of coumarin based naturally occurring compounds was used in medicinal chemistry, such as anticancer, anti-inflammatory, antimicrobial, antioxidant agents, etc.[1,2,3].. Molecular docking study of Coumarin derivatives (2,3-4a,4b,8 and 9) towards the active site of EGFR (PDB ID: 1M17)[4]is performed, predicting binding sites and binding energies with amino acids of receptors.

Inflammation is the body's response to internal and external environment in order to eliminate unwanted agents from the body and thus restore the tissue physiology. Chronic inflammatory conditions in selected organs increase the risk of cancer so inflammation plays an important role in the development of cancer and promotes all stages of tumorigenesis [5,6]. Epidermal Growth Factor Receptor (EGFR) plays an important role in inflammation as well as cancer. EGFR belongs to the Human Epidermal Growth Factor (HER) family of receptors, in which EGFR is activated by binding to EGF which causes receptor dimerization and tyrosine autophosphorylation, leading to cell proliferation [7]. A high level of EGFR kinase enzyme is overexpressed in several tumours such as those in colon, prostate, breast, HeLa, HepG2, and non-small lung cancers [8,9].

The inhibition of EGFR kinase enzyme is used in cancer treatment and is effected by blocking this enzyme with small molecules approved by the FDA such as erlotinib, neratinib, sorafenib, and crizotinib [10]. Additionally, chromines are a major class of widespread products and constitute the core structure of many drugs covering a wide range of biological applications, including EGFR inhibition as well as antitumour activities [11].

Docking simulations of the most active compounds were carried out to give structural insights into the binding mode with epidermal growth factor receptor tyrosine kinase (EGFR TK) [12,13] to illustrate the antiproliferative activities against the HepG2 cancer cell line. Molecules designed to block EGFR TK, a class of potent, selective, ATP-competitive inhibitors of

*Corresponding author e-mail: *eldebss@sci.cu.edu.eg* ; *taha_eldebss@yahoo.com* ; (Taha. M. A. Eldebss)
Receive Date: 10 January 2025, Revise Date: 10 February 2025, Accept Date: 20 February 2025
DOI: 10.21608/ejchem.2025.351834.11140

EGFR TK, induced signaling on their own and further degraded to a DNA-damaging species, which should induce significant cell-killing in tumours [14].

The first molecular probe designed to verify the combitargeting postulates was shown to strongly block the EGFR TK activity on its own in a short exposure enzyme assay [15]. The receptor protein tyrosine kinases play a key role in signal transduction pathways that regulate cell division and differentiation. The interaction of growth factors with these receptors is a necessary event in the normal regulation of cell growth. However, under certain conditions, as a result of overexpression, mutation, or coexpression of the ligand and the receptor, these receptors can become hyperactivated and induce uncontrolled cell proliferation [16].

Among the growth factor receptor kinases, EGFR kinase (also known as erb-B1 or HER-1) is important in cancer deregulation of growth-factor signaling due to hyperactivation of EGFR, which is seen in several cancer types [17,18]. Activation of EGFR might result from overexpression, mutations leading to constitutive activation, or autocrine expression of the ligand. EGFR overexpression is often seen in various cancers [19]. Compounds that inhibit the kinase activity of EGFR after binding to its cognate ligand are of potential interest as new therapeutic antitumor agents [20,21].

Our research objective is to study novel synthesis of new multi-targeting potential Coumarin derivatives compounds towards Epidermal Growth Factor Receptor (EGFR) (PDB ID: 1M17) [4], molecular geometry, electronic properties, and substituent effects of selected Coumarin derivatives using high-level hybrid DFT functional methods of calculations. The study aims to perform molecular docking of multi-targeting proposed inhibitors towards the active site of EGFR (PDB ID: 1M17) to explore the binding sites and binding energy.

The pharmacological relevance of potential derivatives as drugs will be evaluated to establish a correlation between physicochemical properties and their appropriateness as EGFR inhibitors drugs. We aim to explore the relative stabilities of the protein-ligand complexes interactions and screen a set of compounds for further binding energy interaction calculations of the protein-ligand complex with receptor (1M17). With in-depth understanding, the most promising potent inhibitors will be identified.

The selected compounds were evaluated using in silico local and global reactivity, molecular docking. To investigate the dynamics, conformational stability, and structural stability of protein–ligand complexes, molecular dynamics simulations were performed for a long run of 100 ns, followed by computation of the binding free energy of the simulated complexes (1M17-4b and 1M17-9) based on molecular dynamics (MD) simulation results by GROMACS using snapshots taken from the systems' trajectories (100 ns).

TCM[1], with annual consumption at 3.75 TCM. Raw gas requires treatment for effective processing in GTP[2], NGL[3], and LNG facilities[4]. Inorganic impurities in NG streams from wells pose operational challenges, necessitating gas sweetening[5]via adsorption and absorption[6]. Increasing energy demands and stricter regulations related to concession agreements, GSAs, contracts for NG[7,8], LCD, gas market activities[9], gas – hubs[10,11], and gas regulators [12]emphasize the need for efficient gas processing technologies (GSUs) including (AGRU[13], DHU[14], MRU[15], HCDPU[16]) andCCUS (GTL) that reduce costs while ensuring .

Results and Discussion

Chemistry

3-(2-Aminothiazole-4-yl)-2H-chromen-2-one (2) was obtained via the reaction of 3-(2-bromoacetyl)-2H-chromen-2-one (1) with thiourea. The structure of latter product was established on the basis of its elemental analysis and spectral data (Scheme 1). IR spectrum of compound 2 exhibited three bands at 3420 , 3012 and 1720 cm-1 due to NH2 and a carbonyl groups, respectively,(–N=C-N) 1231. Its 1HNMR spectrum displayed three singlet signals at 6.6, 7.7 and 5.2 ppm corresponding to 5CH thiazole , 4CH chromen-2-one and NH2 protons, respectively.

In addition to a multiplet at 7.0 - 7.27 ppm assigned to aromatic protons. Its mass spectrum revealed a peak at m/z 244 due to its molecular ion (Scheme 1).

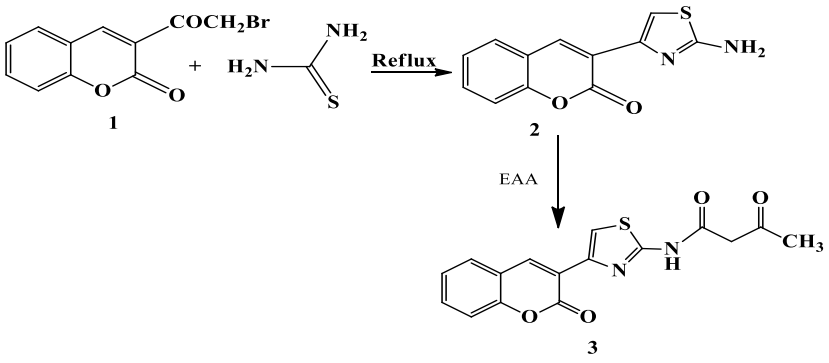

Scheme 1

Treatment of compound 2 with ethyl 3-oxobutanoate afforded a product identified as 3-oxo-N-(4-(2-oxo-2H-chromen-3-yl)thiazol-2-yl) butanamide (3) whose structure was established on the basis of its elemental analysis and spectral data (Scheme 1). The IR spectrum of compound 3 revealed three bands at 1720, 1627 and 1604 cm^{-1} due to three carbonyl groups functions , NH at 3437 and (=C-H) aromatic 1608 ,1589. Its 1HNMR spectrum displayed five singlet signals at 6.6,

8.1 ,7.8 ,3.4 and 2.5 ppm corresponding to 5CH thiazole , 4CH chromen-2-one , NH, CH2 and CH3 protons, respectively. In addition to a multiplet at 7.0 - 7.27 ppm assigned to aromatic protons. Its mass spectrum exhibited a peak at m/z 328 corresponding to its molecular ion.

Compound 3 underwentthree pots cyclocondensationreaction with 4-(dimethylamino)benzaldehyde (or 3-hydroxybenzaldehyde) and urea to afford 1,2,3,4-tetrahydropyrimidine-5-carboxamidederivatives 4a,b (Scheme 2).

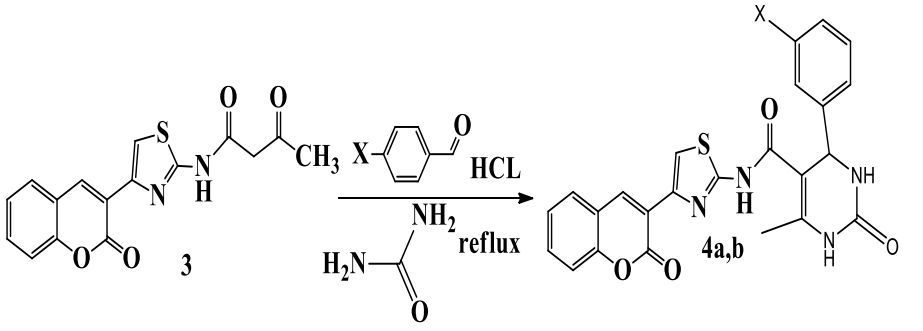

Scheme 2

1

Thus, the IR spectrum of compound (4a) revealed two absorption bands at 3312 and 3374 cm^{-1} due to two NH functions and three absorption bands at 1728,1750, 1770 cm^{-1} due to three carbonyl functional groups whereas its ^1H NMR spectrum showed the lack of signal due to methylene protons, signal at 8.2 corresponds to (–NH amide)6.6 for CH thiazole, (7.0,7.1, 7.2) signals for benzene ring and its mass spectrum showed a peak at m/z 501 corresponding to its molecular ion that supported the proposed structure. 5-(3-(dimethylamino)phenyl)-7-methyl-N-(4-(2-oxo-2H-chromen-3-yl)thiazol-2-yl)-3,5-dihydro-2H-oxazolo[3,2-a]pyrimidine-6-carboxamide (**4a**)

Also, the structures of the isolated cycloadduct 4b was confirmed on the basis of its elemental analyses and spectral data. For example the IR spectrum of the isolated product 4b revealed seven signals at cm−1 3336,3201, 3074, 2966 ,1720,1750,1740,1683 and 1523 N-H, O-H, aromatic C-H, 3(C=O), aliphatic C-H, amide and C=N, respectively.

Its MS, exhibited a band at m/z; 474.5 due to its molecular ion while its ^{1}HNMR revealed four signals at 8.2,6.6, due to NHprotons and NH for urea , signal 2.1 at due to methylene protons, a multiplet in the region δ 7.23 -7.61 , 7.82 corresponding to aromatic protons The structure of the isolated product was confirmed from its spectroscopic as well as its elemental analytical data (See Experimental part).

Treatment of 4-(3-dimethylamino)phenyl)-6-methyl-2-oxo-N-(4-(2-oxo-2H-chromen-3-yl) thiazol-2-yl)-1,2,3,4-tetrahydropyrimidine-5-carboxamide **4a** with acetic anhydride afforded 1-acetyl-6-(3-(dimethylamino)phenyl)-4-methyl-2-oxo-N-(4-(2-oxo-2H-chromen-3-yl)-1,2,3,6-tetrahydropyrimidine-5-carboxamide (**8**) on the basis of its elemental analysis and spectral data

The structure of latter product **8** was established on the basis of its elemental analysis and spectral data (Scheme 3). IR spectrum of compound **8** exhibited seven bands at 3479 , 3182, 2927, 1720,1735,1770 and 1620 cm-1 due to NH, CH aromatic ,CH aliphatic 3-carbonyl and a C=N groups, respectively. Its 1HNMR spectrum displayed three singlet signals at 7.5, 8.1 and 7.1 ppm corresponding to 5CH thiazole , 4CH chromen-2-one and NH2 protons, respectively. In addition to a multiplet at 7.0 - 7.27 ppm assigned to aromatic protons. Its mass spectrum revealed a peak at m/z MS, m/z; 543.5 due to its molecular ion (Scheme 3).

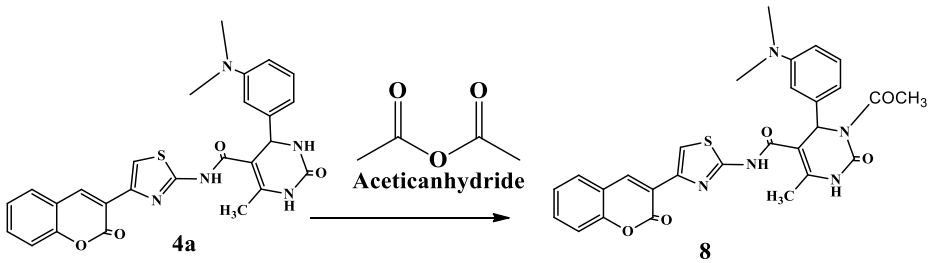

Scheme 3

Treatment of 4-(3-dimethylamino)phenyl)-6-methyl-2-oxo-N-(4-(2-oxo-2H-chromen-3-yl) thiazol-2-yl)-1,2,3,4-tetrahydropyrimidine-5-carboxamide **4a** with p-toluene sulphonic acid afforded4-(6-(3-(dimethylamino)phenyl)-4-methyl-2-oxo-5-((4-(2-oxo-2H-chromen-3-yl)thiazol-2-yl)carbamoyl)-2,3-dihydropyrimidin-1(6H)-yl)benzenesulfonic acid (**9**) on the basis of its elemental analyses and spectral data.Thus, IR Spectrum of compound **9**revealed seven absorption bands at 3479, 3120, 2927,1724,1760, 1775and1646 cm^{-1} due to NH, aromatic C-H, aliphatic C-H functions,3carbonyl group andC=N functional groups whereas its 1H NMR spectrum showed 8.4, 7.0-7.24, 6.5-6.8 and 6.6its mass spectrum showed a peak at m/z 657corresponding to its molecular ion that supported the proposed structure (Scheme 4).

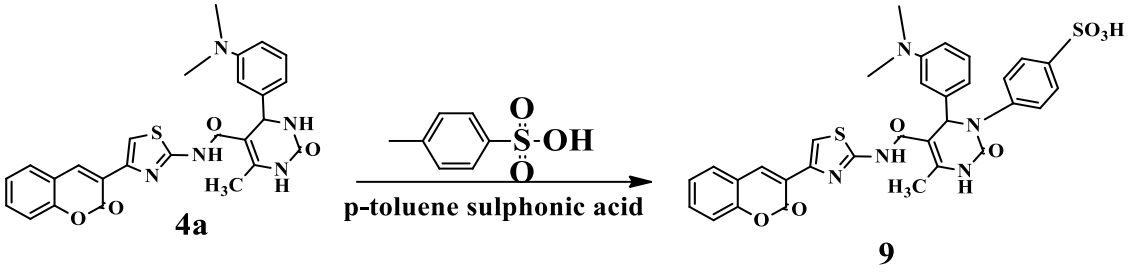

Scheme 4

Experimental Section

A series of coumarine derivatives were synthesized through 4 schemes. All the compounds gave satisfactory chemical analysis. The chemical structures of these compounds were determined by IR ,1H-NMR, mass spectrometry (ESI-MS) spectra and elemental analyses.

All chemicals (reagent grade) used in the experiment were purchased from Sigma Aldrich, all melting points were measured on a Gallenkamp melting point apparatus. The infrared spectra were recorded in potassium bromide disks on a Pye Unicam SP 3300(Pye Unicam Ltd., Cambridge, UK) and Shimadzu FT IR8101 PC (Schimadzu, Tokyo, Japan) infrared spectrophotometers.The NMR spectra were recorded on a Varian Mercury VX-300NMR spectrometer. 1H (300 MHz).Chemical shifts were related to that of the solvent. Mass spectra were recorded on a Shimadzu GCMS-QP 1000 EX mass spectrometer (Schimadzu) at 70 eV. Elemental analyses were carried out at the Microanalytical Center of Cairo University, Giza, Egypt.

3-(2-aminothiazole-4-yl)-2H-chromen-2-one(2)

To a solution of 3-(2-bromoacetyl)-2H-chromen-2-one (26.70 g, 0.1 mol) in ethanolwas added thiorea (7.6 g, 0.1 mol). The reaction mixture was refluxed for 8 h then allowed to cool. The reaction mixture poured onto cold water with continuous stirring and scratching. The solid product was collected by filtration, washed with water, dried, and finally recrystallized fromethanol to afford the corresponding product in 90% yield, m.p. : 350–351 °C, IR (KBr) ν (cm−1) = 3420 (N-H str), 1720,(C=O),3012 (aromatic C-H),2935 (aliphatic C-H),MS, m/z; 244 (M+, 100%), 237(89%), 207 (73%), 85 (118%),246 (67%),180 (57%), 1HNMR (DMSO-d6)δ (ppm) = 4.0 (s,1H),6.6 (s, 1H), 7.0 -7.27 (s,5H). For **$C_{12}H_8N_2O_2S$** (244.27), Calcd.: C: 59.00;H: 3.30; N: 11.47; O: 13.10; S: 13.3%. Found: C: 58.97; H : 3.35; N:11.49; O: 13.08; S: 13.4%.

3-oxo-N-(4-(2-oxo-2H-chromen-3-yl) thiazol-2-yl) butanamide (3)

To a solution of 3-(2-aminothiazole-4-yl)-2H-chromen-2-one(start) (24.4 g, 0.1mol) in ethanol was added ethyl 3-oxobutanoate (13.01 g, 0.1mol). The reaction mixture was refluxed for 30 min. then allowed to cool. The reaction mixture poured onto cold water with continuous stirring and scratching. The solid product was collected by filtration, washed with water, dried, and finally recrystallized from ethanol to afford the corresponding product in 87% yield, m.p.: 528–530 °C, IR (KBr) ν (cm−1) = 3360, (N-H str), 1720,(C=O),1627,1604 (C=O), 3012 (aromatic C-H),2935 (aliphatic C-H),1563 (C= N). MS, m/z; 244 (M+, 100%), 177 (80%), 207 (73%), 332 (64%), 269 (52%), 60 (43%) 1HNMR (DMSO-d6)δ (ppm) = 8.1 (s, 1H), 2.4(s, 1H), 3.3(s, 1H), 6.6(m, 1H) 6.9-7.8 (5H). For **$C_{16}H_{12}N_2O_4S$** (328.34), Calcd.: C: 58.53;H: 3.68; N: 8.53; O: 19.49; S: 9.77%. Found: C: 58.50; H: 3.60; N: 8.50; O: 19.41; S: 9.75%.

4-(3-dimethylamino)phenyl)-6-methyl-2-oxo-N-(4-(2-oxo-2H-chromen-3-yl) thiazol-2-yl)-1,2,3,4-tetrahydropyrimidine-5-carboxamide(4a)

To a solution of 3-oxo-N-(4-(2-oxo-2H-chromen-3-yl) thiazol-2-yl) butanamide(32.8 g.0.1 mol) and4-(dimethyl amino)benzaldehyde (14.9 g, 0.1 mol) in ethanol was added Urea (6 g, 0.1 mol) and drops of conc.HCl was added. The reaction mixture was refluxed for 8 hrs then allowed to cool. The reaction mixture poured onto cold water with continuous stirring and scratching. The solid product was collected by filtration, washed with water, dried, and finally recrystallized from ethanol to afford the corresponding product in 88% yield,m.p.: 910–912 °C, IR (KBr) ν (cm−1) = 3312, (N-H str), 1728,(C=O),3174 (aromatic C-H),2924 (aliphatic C-H),+ MS, m/z; 501 (M+, 98%), 175(90%), 305 (42%), 478 (24%), 59 (43%), 1HNMR (DMSO-d6)δ (ppm) = 2.4(s, 1H), 2.8(s, 2H), 6.6(s, 1H), 9(s, 1H),7.1-7.4 (s,4H). For **$C_{26}H_{23}N_5O_4S$** (501.5), Calcd.: C: 62.26;H: 4.62; N: 13.96; O: 13.96; S: 6.39%. Found: C: 62.60; H: 4.65; N: 13.95; O: 13.98; S: 6.35%.

4-(3-hydroxyphenyl)-6-methyl-2-oxo-N-(4-(2-oxo-2H-chromen-3-yl) thiazol-2-yl)-1,2,3,4-tetrahydropyrimidine-5-carboxamide(4b)

To a solution of 3-oxo-N-(4-(2-oxo-2H-chromen-3-yl) thiazol-2-yl) butanamide(32.9 g, 0.1 mol) in ethanol was added Urea (6 g, 0.1 mol) and 3-hydroxybenzaldehyde (12.2 g,0.1 mol)and drops of Conc.HCl. The reaction mixture was refluxed for 8 h then allowed to cool.The reaction mixture poured onto cold water with continuous stirring and scratching. The solid product was collected by filtration,washed with water, dried, and finally recrystallized from ethanol to afford the corresponding product in 90% yield,m.p.: 945–955 °C, IR (KBr) ν (cm−1) =3201 (O-H), 3336, (N-H str), 1720,(C=O),3074 (aromatic C-H),2966 (aliphatic C-H),1523 (C=N),1683 (amide), MS, m/z; 474.5 (M+, 80%), 63(83%), 398 (45%), 260 (63%), 459 (37%), 1HNMR (DMSO-d6)δ (ppm) =8 (s, 1H), 5.3(s, 1H), 6.6(s, 1H),7.0-7.27 (s, 4H). For **$C_{24}H_{18}N_4O_5S$** (474.5), Calcd.: C: 60.75;H: 3.82; N: 11.83; O: 16.86; S: 6.76%. Found: C: 60.73; H : 3.85; N:11.81; O: 16.88; S: 6.74%.

1-acetyl-6-(3-(dimethylamino)phenyl)-4-methyl-2-oxo-N-(4-(2-oxo-2H-chromen-3-yl)-1,2,3,6-tetrahydropyrimidine-5-carboxamide(8)

To a solution of 4-(3-dimethylamino)phenyl)-6-methyl-2-oxo-N-(4-(2-oxo-2H-chromen-3-yl) thiazol-2-yl)-1,2,3,4-tetrahydropyrimidine-5-carboxamide(50.1 g, 0.1 mol) in aceticanhydride. The reaction mixture was refluxed for 8 h then allowed to cool.The reaction mixture poured onto cold water with continuous stirring and scratching. The solid product was collected by filtration,washed with water, dried, and finally recrystallized to afford the corresponding product in 90% yield, m.p.: 913–914 °C, IR (KBr) ν (cm−1) = 3479, (N-H str), 1724,(C=O),3182 (aromatic C-H),2927 (aliphatic C-H),1546 (C=N), MS, m/z; 543.5 (M+, 98%), 532(94%), 517 (60%), 515 (45%), 59 (43%), 1HNMR (DMSO-d6)δ (ppm) = 6.5-6.8(S,4H),2.8(s, 2H), 8.0(s, 1H), 6.6(s, 1H), 7.0-7.24(s, 4H). For **$C_{28}H_{25}N_5O_5S$** (543.5), Calcd.: C: 61.87;H: 4.64; N: 12.88; O: 14.72; S: 5.90l%. Found: C: 61.85; H: 4.63; N: 12.83; O: 14.75; S: 5.88%.

4-(6-(3-(dimethylamino)phenyl)-4-methyl-2-oxo-5-((4-(2-oxo-2H-chromen-3-yl)thiazol-2-yl)carbamoyl)-2,3-dihydropyrimidine-1(6H)-ylbenzene sulphonic acid(9)

To a solution of 4-(3-dimethylamino)phenyl)-6-methyl-2-oxo-N-(4-(2-oxo-2H-chromen-3-yl) thiazol-2-yl)-1,2,3,4-tetrahydropyrimidine-5-carboxamide(50.1 g, 0.1 mol) in ethanol and triethylamine(TEA)was added P-toluene sulphonic acid (17.2 g, 0.1 mol) The reaction mixture was refluxed for 6 hrs then allowed to cool.The reaction mixture poured onto cold water with continuous stirring and scratching. The solid product was collected by filtration,washed with water, dried, and finally recrystallized from ethanol to afford the corresponding product in 90% yield,m.p.: °C, IR (KBr) ν(cm−1) =3340(O-H), 3421, (N-H str), 1724,(C=O),3186 (aromatic C-H),2924 (aliphatic C-H),1523 (C=N),1684 (amide), MS, m/z; 657.7 (M+, 99%), 532(94%), 517 (60%), 515 (45%), 59 (43%), 1HNMR (DMSO-d6)δ (ppm) =1.8 (s,H), 6.5-6.8(S,4H),2.8 (s, 2H), 8.0(s, 1H), 6.6(s, 1H), 7.0-7.24(s, 4H). For **$C_{32}H_{27}N_5O_7S_2$** (657.7), Calcd. : C: 58.44;H: 4.14; N: 10.65; O: 17.03; S: 9.75%. Found: C: 58.42; H : 4.16; N:10.64; O: 17.1; S: 9.73%.

1- Antiproliferative activities assay

Cytotoxicity evaluation using viability assay: For cytotoxicity assay,**Mammalian cell lines: HepG-2** cells (human Hepatocellular carcinoma) and **HCT-116** (colon carcinoma)**MCF-7** breast cancer cell line were obtained from VACSERA Tissue Culture Unit.

Chemicals Used: Dimethyl sulfoxide (DMSO), trypan blue dye were purchased from Sigma (St. Louis, Mo., USA). Fetal Bovine serum, DMEM, RPMI-1640, HEPES buffer solution, L-glutamine, gentamycin and 0.25% Trypsin-EDTA were purchased from Lonza.

Cell line Propagation:

The cells were cultured in Dulbecco's Modified Eagle's Medium (DMEM), which was supplemented with 10% heat-inactivated fetal bovine serum, 1% L-glutamine, HEPES buffer, and gentamycin at a concentration of 50 µg/ml. They were maintained at 37°C in a humidified atmosphere containing 5% CO_2 and subcultured twice weekly. For experiments, cells were plated in 96-well plates at a density of 1×10^4 cells per well in 100 µl of growth medium. After 24 hours, fresh medium containing varying concentrations of the test compound was introduced. Serial two-fold dilutions of the compound were prepared and added to the cell monolayers in flat-bottomed 96-well microtiter plates (Falcon, NJ, USA) using a multichannel pipette. The plates were incubated at 37°C in a humidified environment with 5% CO_2 for 48 hours. Each concentration of the test compound was evaluated in triplicate. Control wells contained cells without the test sample, with or without DMSO. The maximum DMSO concentration (0.1%) was confirmed to have no impact on the assay. Following the incubation period, cells were treated with various sample concentrations for an additional 24 hours, and cell viability was assessed using a colorimetric assay. In brief, the medium was aspirated, and a 1% crystal violet solution was added to each well for at least 30 minutes. Excess stain was washed away with tap water, and the wells were treated with 30% glacial acetic acid to solubilize the dye. Absorbance was measured at 490 nm using a microplate reader (TECAN, Inc.), with background absorbance from unstained wells subtracted. The results were compared to untreated control cells. All experiments were performed in triplicate, and cell cytotoxicity was calculated. Viability was determined based on optical density (OD) using the formula: viability (%) = [1-(ODt/ODc)] × 100%, where ODc represents the mean OD of treated wells, and OD_a refers to the mean OD of control wells. Dose-response curves were plotted to evaluate the survival rate of each cell line after treatment with the compound. The half-maximal inhibitory concentration (IC_{50}), defined as the concentration causing a 50% reduction in cell viability, was derived from these plots using GraphPad Prism software (San Diego, CA, USA). Each experiment was conducted at least three times.

2- EGFR Inhibitory Assay HEPG2 cells lines by ELISA technique:

Principle

The Epidermal Growth Factor Receptor (EGFR) ELISA for humans is a solid-phase sandwich Enzyme-Linked Immunosorbent Assay designed for the quantitative measurement of EGFR protein in cell lysates. The assay uses a monoclonal antibody specific to EGFR, regardless of its phosphorylation state, which is pre-coated onto the wells of the provided multiwell plate. EGFR standards, control samples, and test specimens are added to these wells. During the initial incubation step, the EGFR antigen binds to the capture antibody immobilized on the plate. Following this incubation, unbound components are washed away, and a secondary antibody specific for full-length EGFR is introduced. This detection antibody binds to the immobilized EGFR during the second incubation step. After washing off any unbound detection antibody, a horseradish peroxidase (HRP)-conjugated anti-rabbit IgG (Anti-Rabbit IgG-HRP) is applied. This enzyme-labeled antibody binds to the detection antibody, completing the sandwich complex. After a third incubation and subsequent washing to eliminate excess HRP-conjugated antibody, a substrate solution is added. The enzymatic reaction with the substrate produces a color, the intensity of which correlates directly with the concentration of full-length EGFR in the sample. The absorbance at

450 nm is measured using a microplate reader to determine the EGFR concentration. This assay is specifically designed to detect and quantify full-length human EGFR protein independently of its phosphorylation state. It does not recognize the 110 kDa truncated EGFR variant, which lacks the cytoplasmic tyrosine kinase domain. The assay is suitable for measuring full-length EGFR in cell and tissue lysates and can normalize EGFR content in samples containing EGFR phosphorylated at Tyr1173 and Tyr1068 when used alongside Sigma Phospho-EGFR ELISAs (Product Nos. CS0140 and CS0150).

Buffers preparation

Cell Extraction Buffer was consisted of10 mM Tris (pH 7.4), 100 mM NaCl, 1 mM EDTA, 1 mM EGTA, 1 mM NaF, 20 mM Na4P2O7, 2 mM Na3VO4, 1% Triton™ X-100, 10% glycerol, 0.1% SDS, and 0.5% deoxycholate.and Immediately before use, PMSF was added (0.3 M stock in DMSO) to 1 mM and 50 µL protease inhibitor cocktail (e.g., Sigma Cat. No. P-2714) for each 1 mL of Cell Extraction Buffer.

Samples preparation

This experiment utilized four T75 flasks for compound (9) and another four flasks for the negative control. HepG2 cells were seeded in each flask at a density of 6×10^6 cells/ml using RPMI-1640 supplemented medium and incubated for 24 hours. Subsequently, the medium in each flask was replaced. For the flasks assigned to compound (9), fresh medium containing one of the following concentrations was added: 2 µg/ml, 4 µg/ml, 8 µg/ml, and 16 µg/ml. The control flasks received only fresh medium without the compound. After 48 hours of incubation, the adherent cells were gently rinsed with a moderate amount of pre-chilled PBS and harvested by scraping. The cells were transferred into 15 ml tubes and centrifuged at 1,000 × g for 5 minutes at 4°C. The supernatant was discarded, and the cell pellets were resuspended in ice-cold PBS buffer and washed three times. The PBS buffer (pH 7.4) contained the following components: disodium hydrogen orthophosphate (1.42 g/L), potassium dihydrogen orthophosphate (1.36 g/L), potassium chloride (0.20 g/L), and sodium chloride (6.96 g/L).

Next, the cells were lysed using a cell extraction buffer consisting of 10 mM Tris (pH 7.4), 100 mM NaCl, 1 mM EDTA, 1 mM EGTA, 1 mM NaF, 20 mM $Na_4P_2O_7$, 2 mM Na_3VO_4, 1% Triton™ X-100, 10% glycerol, 0.1% SDS, and 0.5% deoxycholate, supplemented with protease inhibitors. A volume of 1 ml of cell extraction buffer was used for every 10^8 cells. The lysates were pipetted into clean microcentrifuge tubes, vortexed, and incubated on ice for 30 minutes with occasional mixing. To remove cellular debris, the lysates were centrifuged at 15,000 × g at 4°C for 10 minutes. The clarified supernatant was then transferred to new microcentrifuge tubes and stored at -80°C until further use. Before performing the assay, the extracted cell lysate samples containing EGFR protein were diluted at a ratio of at least 1:10 using the Standard Diluent Buffer.

Preparations of Standard dilutions

EGFR Standard

1. Reconstitute one vial of Standard was reconstituted with of Standard
Diluent Buffer according to label directions and mixed gently then allowed to sit for 10 min.
2. Mix gently and wait 10 minutes to ensure complete For complete reconstitution.
3. Labeled as 10 ng/mL EGFR.
4. Prepare serial stand and mixed well in each step.

Table 1

Tube	Standard Buffer	Standard from tube	Final EGFR ng/ml
1.	**Reconstituted according to label instructions**		**10 ng/ml**
2.	**0.25 ml**	**0.25 ml (1)**	**5**
3.	**0.25 ml**	**0.25 ml (2)**	**2.5**
4.	**0.25 ml**	**0.25 ml (3)**	**1.25**
5.	**0.25 ml**	**0.25 ml (4)**	**0.625**
6.	**0.25 ml**	**0.25 ml (1)**	**0.312**
7.	**0.25 ml**	**0.25 ml (1)**	**0.16**
8.	**0.5 ml**	**-----**	**0**

Anti-Rabbit IgG-HRP Concentrate (100X),

Contains 50% glycerol is very viscous, Equilibrated to room temperature, mixed gently and pipette slowly ,excess concentrate solution from pipette tip was removed tip with clean absorbent paper

Mix: 10 mL IgG-HRP concentrate was mixed with 1 mL HRP Diluent.

Wash Buffer

1. Equilibrated to room temperature and mixed to redissolve any precipitated salts.
2. 1 volume Wash Buffer Concentrate 25X was mixed with 24 volumes of deionized water
3. Labeled as **Working Wash Buffer.**

Assay Procedure (Total time 4 hr)

1- 100 µL Standard Diluent was added to zero wells, 100 µL standards, diluted cell extract samples or controls were added to the appropriate wells. Tap gently on the plate was taped gently to mix, coverd with Plate Cover and

incubated 2 hours at room temperature. Then wells were washed 4 times by washing buffer using manifold pipette tap dry on absorbent tissue.

2- 100 µL Anti-EGFR (detection) antibody was added to all wells (except chromogen blanks). After the final wash blot dry on a lint free paper towel to remove any remaining wash buffer the plate was taped gently to mix, covered with Plate Cover and incubated 1 hour at room temperature. Wells were washed for a total of 4 times as instruction, After the final wash blot dry on a lint free paper towel to remove any remaining wash buffer.

3- 100 µL Anti-Rabbit IgG-HRP Working Solution was added to each well except the chromogen blanks. Plate covered with plate cover and incubated 30 minutes at room temperature. wells were washed for a total of 4 times. After the final wash blot dry on a lint free paper towel to remove any remaining wash buffer.

4- 100 µL of Stabilized Chromogen was added into all wells. *The liquid in the wells will begin to turn blue. The plate* Incubated approximately 30 minutes at room temperature in the dark without covering the plate

5- 100 µL of Stop Solution was added to each well. This stops the reaction m the plate was Taped gently to mix. *The solution will turn yellow.*

6- Absorbance was red at 450 nm within 2hrs after addition of stop solution and the plate was blanked against chromogen i.e Blank wells contain chromogen and stop solution only).

Results

The concentrations of EGFR calculated as follows:

1. Calculation the Average Net OD (nm) for each standard dilution and samples

Average Net OD (nm) = Average Bound OD (nm) – Average Chromogen Blank OD

2. On graph paper the Average Net OD (nm) of standard dilution (nm) was plotted against the concentration (ng/mL) of EGFR for the standards.

3. the best curve was draw through these points to construct the standard curve.

4. The EGFR concentrations in unknown samples and controls determined by interpolation from the standard curve.

5. The values obtained for the samples were multiplied by dilution factor of each sample.

2. Computational Details

2.1 Density functional theory (DFT)calculations

During this study, packages of programs are used to run the molecular modeling calculations of antimicrobial inhibitors of seven potential target derivatives**(2,3-4a,4b,8 and 9)**were carried out using *Gaussian09W* software package **[22]**. The molecular geometry of target Coumarinderivatives was fully optimized usingdensity functional theory with the Becke's three parameter exchange functional and the gradient corrected functional of Lee, Yang and Parr (DFT/B3LYP) **[23–26]** using largest basis set 6-311++G (d, p).The choice of hybrid functional B3LYPwith a large basis set6-311++G (d, p) **[27]** was due to accuracy, consistent,flexibility, better performance and good correlation experimental. During the geometry optimization, no symmetry constrains were applied **[28,29]**.The same level of theory has been applied to compute vibrational frequencies for each compound, and the molecular structure of target compounds were found correspond to real minima of the potential energy surface. In order to identify the reactive site of the molecules, the DFT/B3LYP were employed to describe reactivity descriptors and molecular stability. A descriptor of local reactivity was computed using the Fukui function and the Dual descriptor **[30-36].**

Furthermore, the quantum chemical descriptors fromConceptual density functional theory (**CDFT**)were calculated by utilizing the Multiwfn v3.8 software program**[37]**.The electrostatic potential (ESP) of the molecules was rendered by the Visual Molecular Dynamics package (VMD 1.9 program) based on the data outputted by the Multi fnprogram **[37,38]**. Natural Bond Orbital (NBO) analysis have been calculated utilizingNBO 3.1 which is provided in the Gaussian 09W program. The GaussView (v6.1) **[39]**and ChemCraft (v1.6) package**[40]**were used to visualize the optimized structure andmolecular orbitals. The QSAR features included in the HyperChem program (v8.0.7) **[41]**were used to determine the SAR properties of all target compounds.

2.2 Molecular Docking simulation

The 3D structures of all synthesized hybrids of Coumarin derivatives **(2,3-4a,4b,8 and 9)**were previously geometry optimized using B3LYP/6-311++G(d,p) level of theory and then saved in *PDB* file format.

The protein structure was prepared for molecular docking study according to our previous studies and saved in PDB format. Finally, molecular docking simulation was performed as previously reported **[42].** visualization and analysis were generated in the Discovery Studio Visualizer software (windows v21.1.0.20298) **[43]**to draft 2D and 3D figures of ligand-receptor complex structures indicating such interactions.

2.3 Molecular Dynamics simulation (MDS)

The both top consensus docking scores from target compounds**(2,3-4a,4b,8 and 9)**with protein receptor(**1M17)**were advanced to all-atom MD simulations to study the relative stabilities of the protein-ligand interactions and screen compound for further binding energy calculations. All the simulations were done using the GROMACS V2020package **[44–46]**and the CHARMM**[47]** force field, the parameters and topological files for the selected compounds were generated using the latest CHARMM/CGenFF force field through CHARMM-GUI **[48–51].**The protein–ligand complex was immersed in the center of a box of solvated water molecules with a TIP3P explicit solvation model 0.15 M ions (182 Na^+ and 174Cl^-); to mimic the physiological salt concentrations; were added to provide charge neutralization and electrostatic screening which extended 20Å

from the protein. CHARMM and the periodic boundary conditions were set with dimensions of rectangle cubic system 126.0, 126.0, and 126.0 Å in x, y, and z directions, respectively.

The MD protocols involve minimization, equilibration, and production. no atoms were restrained in the 100 ns MD production simulations. The isothermal–isobaric (NPT) ensemble and a 2.0*fs* time integration step were chosen for all MD simulations. Through the 100 ns of MD production, the pressure was set at 1 atm using the Nose´–Hoover Langevin piston barostat **[52,53].** The temperature was set at 300.0 K using the Langevin thermostat.**[54].**For the minimization and equilibration of the complexes in the water box, we assumed force-field parameters excluding scaling of 1.2 nm. All atoms, including those of hydrogen, were illustrated explicitly. Complexes preliminary energy was minimized via 5000 steps at constant temperature (300 K), followed bythe solvated protein–ligand complex system was equilibrated with 1,000,000 steps with time integration step 1.0*fs* for minimization and equilibration and 50,000,000 runs for 100 ns with time integration step 2.0 *fs*. The structural coordinates were kept every 25 ps into the trajectories. The generated trajectories recovered from the production step were utilized to analysis of the whole system residues by using tools implement in the GROMACS and VMD package **[38]**. A distance cut-off of the short-range neighbor list 1.0 nm was applied to short-range nonbonded interactions with a pair list distance of 1.2 nm, and Lennard Jones interactions were smoothly truncated at 1.2 nm (rvdm, rcoulomb = 1.2 nm). Long-range electrostatic interactions were treated using the particle-mesh Ewald (PME) method **[55,56],**where a grid spacing of 1.0 Å was used for all simulation cells. For consistency, we have applied the same protocol for all MD simulations.

2.4 Binding Free Energy Calculations

The binding free energy of both the best simulated complexes (**1M17- 4b and 1M17- 9)** were computed based on molecular dynamical (MD) simulated results by GROMACSusing snapshots taken from the systems trajectories (100 ns) follow by gmx_MMPBSA tool based on AMBER tools MMPBSA.py module with GROMACS files **[57]** in which the ligand (*L*) binds to the protein receptor (*R*) to form the complex (*RL*). we are only interested in relative binding energies calculations, which are the Gibbs relative binding energy is given by:

$$\Delta G_{bind} = \Delta G_{bind,\ vaccum} + \Delta G_{RL,\ Solvation} - (\Delta G_R - \Delta G_L)$$

Biological activity

The in vitro antiproliferative activities of the synthesized coumarine derivatives (**2,3,4a,4b.8,9)** were studied using the human liver cancer cell line HepG2, human colon cancer cell line Hct116 and human breast cancer cell line MCF-7 by the following method and the compounds were tested with a range of concentration and the IC50 values was calculated i.e. the concentration(μM) of compounds which were able to cause 50% of cell death with respect to the control culture.

Compounds found to show a potent activities with IC50 values range from 4.1 and 27.3 μM, respectively. Compounds **3**, **4(b)**, **9,** showed the best antiproliferative activities with IC50 values 8.8,6.4and 4.1 Mm respectively for HepG2 cell line. The remaining compounds showed less antiproliferative activities with IC50 values ranging from 10.7-15.7 μM when compared to doxorubicin and vinblastin as Positive control also the previous compounds shows their antiproliferative effect for HCT 116 cell line with IC50 range from 5.3- 27.6 μM and compound **3,6 ,9**showed the best antiproliferative activities and the remaining compounds shows less antiprolifrative activity to human colon cancer cell line.**as shown in (Table 2).**

Compound **3,9** shows high and the best antiproliferative activity when tested for human breast cancer cell line with **IC50 3.4,10.9** repectively and the remaining compound shows less potent activity. **as shown in (Table 2) and Fig 1.**the most active in all tested three cell lines was Compound **9** evaluated for their ability to inhibit the autophosphorylation of EGFR kinases using a solid-phase ELISA assay the synthesized compound showed potent EGFR inhibitory activities.

The results showed the same trends for antiproliferative activities against Hep-G2 as EGFR was an important factor in liver cancer.. Here, again, compound **9** showed the most potent inhibitory activities (IC50 = 4.1 μM), and was comparable to the positive control doxorubicin (IC_{50} = 2.1 μM)and vinblastin (IC50=4.6 μM) . as shown in Fig:

The four chromine derivatives compounds, allowed to molecular docking studies demonstrated that almost all the compounds showed the best activity both in the antiproliferative activities against Hep-G2 cell line and for EGFR inhibition. The results indicated that the hydroxyl phenyl group substituent at the 4-position in pyrimidine moiety could significantly increase the activity. Also substitution sulphonic acid in position 1 and its toutomer in pyrimidine ring shows more inhibitory effect and more antiproliferative effect to EGFR. However, the SAR result summarised above was a brief overview of the whole 4 compounds synthesised, Docking simulations suggested that compound **9** had a good binding activity with EGFR kinase, and due to its chemical structure **9** also a good EGFR inhibitor, and thus had good antiproliferative activity against *Hep-G2.*

Table 2: Cytotoxicities of target compounds 2-9 against various cancer cell lines.

Compound no.	Invitro cytotoxicity IC_{50}[a] (μM)		
	$HepG_2$[b]	HCT 116[b]	MCF-7[b]
2	**10.7**	**27.6**	**33.8**
3	**8.8**	**12.4**	**10.9**
4(a)	**11.8**	**13.7**	**27.8**
4(b)	**6.4**	**15.1**	**33.6**
8	**12.8**	**22.4**	**23.9**
9	**4.1**	**5.3**	**3.4**
Duxurubcin[c]	**2.1**	**0.469**	
Vinblastine[c]	**4.6**		**4.6**

A IC_{50}: Compound concentration required to inhibit tumor cell proliferation by 50%.

B Abbreviations: HepG2: human hepatocellular liver carcinoma cell line; MCF-7: human breast adenocarcinoma cell line.

C Used as a positive control

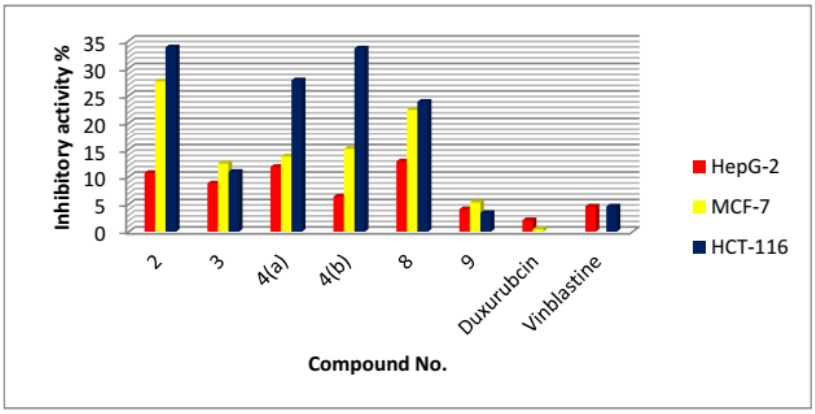

Figure (1): Diagram showed the IC_{50} values (the drug concentrations that inhibited 50% of cell proliferation) of the tested compounds 2-9 on the three cell lines MCF7, HCT116, and HEPG2 after 48 hr exposure

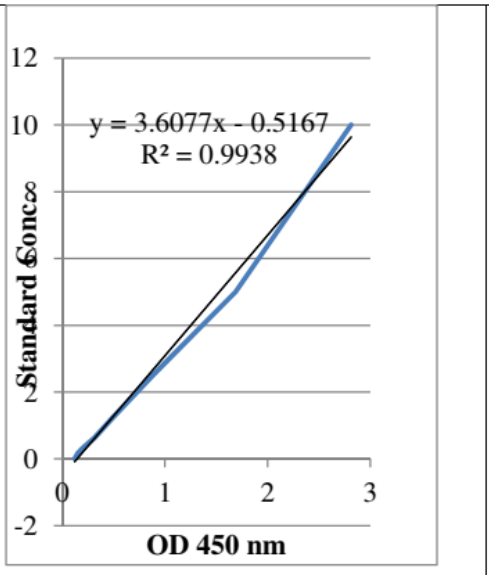

Figure (2): Diagram showed the standared curve values of Human EGFR

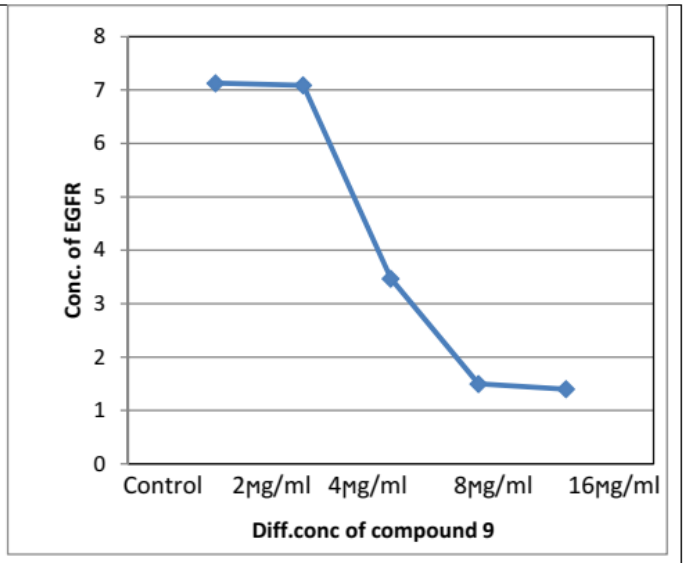

Figure (3): Diagram showed the inhibitory effect of compound 9 on EGFR.

Binding Mode of 3,4(b), 9 derivatives with EGFR Kinase

Molecular docking for synthesized compounds from **(2,3,4,8,9)** to give structural insight and explanation to enzyme – ligand interaction and understanding of good activity.

Compounds docked into the ATP binding site of EGFR, X-ray structure of epidermal growth factor receptor tyrosine kinase domain 2 in complex with 4-anilinoquinazoline inhibitor erlotinib(PDB:1M17) **[21]** was downloaded from protein data bank was performed using the automated moe MOE 2014.0901docking tools **[58].**

The binding mode with aminoacids of all compounds showed in **Table (3)** and the binding model of most active compounds 3,4(a), and 9 was illustrated were depicted in **Figures 4,5,and 6.** Docking studies of four compounds into the active site of EGFR provided well clustered solutions. In the binding model of compound **3** and EGFR, there was a 9 hydrogen bond with total binding energy of **(-11.3 K cal/mol)** a strong hydrogen bond between the carbonyl oxygen no.6 and amino acid **LYS 721** also H bond interaction between the Lys831and S 32 moreover, 2 Cation-π interactions with Leu 694 and another Cation-π interaction with 772 was also observed. Cation-π interaction is known as a noncovalent molecular interaction between the face of an electron-rich π system with an adjacent cation. This unusual interaction is an example of noncovalent bonding between a monopole (cation) and a quadrupole (π system). Cation-π interaction energies are of the same order of magnitude as hydrogen bonds or salt bridges and play an important role in molecular recognition **[59].** Molecular docking studies of compound **4(b)** shows 8 hydrogen bonds with total binding energy of **(-14.7 K cal/mol)** 2 strong hydrogen bonds between carbonyl 5 and **LYS 721 and carbonyl in chromene group also between OH group with Met742** Cation-π interaction and pi-H Bonds also found with **Lys 721.**

Finally, Molecular docking of compound **9 shows 10 hydrogen bond with total binding energy of 16.4 K cal/mol).**

compound 9 shows in docking a strong H bond between Lys 642 and O 42 in sulphonic acid group and another ionic bond between the same residue and pi –H interactions between leu 694,Thr 766,Cys 773,Leu 820. Cation-π interaction, H and ionic bonds made the **9**/EGFR kinase complex more stable.

Table (3): List of docking ligands against EGFR with the score and interacting amino acid

Compound no.	Total binding energy E (Kcal/mol)	No.of H-bonds	Interacting residues
2	-3.4	7	GLU 738 MET 742 MET 742 LEU 694 VAL 702 VAL 702 GLY 772
3	-11.3	9	THR 830 ASP 831 LYS 721 LEU 694 LEU 694 LEU 694 VAL 702 VAL 702 GLY 772
4(a)	-5.1	5	ASP 831 MET 769 CYS 773 LEU 694 GLY 772
4(b)	-14.7	8	MET 742 GLU 738 MET 742 LYS 721 LYS 721 PHE 699 LYS 721 LYS 721
8	-3.7	8	GLU 738 MET 742 MET 769 VAL 702 LYS 721 GLY 772 GLY 772 LEU 820
9	-16.4	7	MET 769 CYS 751 GLY 772 LYS 692 LYS 692 LEU 694 THR 766 CYS 773 CYS 773 LEU 820

3.1. Structural Activity Relationships (SAR)

In this study, the physicochemical properties such as molar volume (V), hydration energy(HE), molar refractivity (MR), surface area grid (SAG) and polarizability (Pol) for targeting hybrid Coumarin derivatives(2,3-4a,4b,8 and 9) were calculated (Table 3) and discussed using HyperChem (v8.0.7). Themolecular polarizability (Pol) characteristics of a compound are determined based on howefficiently its electronic system would control itself in response to the presence of anexternal electric field of light. The importance of molecular polarizability is that it playsa crucial role in simulating a variety of compound characteristics and bioactivities [60].Molecule volume, which controls things like blood-brain barrier permeability andintestinal absorption, is the main factor that influences molecular polarizability. Thus,molecular volume must be used in QSAR investigations to simulate molecularcharacteristics andbioactivities. A further SAR parameter is molar refractivity (MR), asteric characteristic that is dependent on the spatial arrangement of the phenyl ring in thecompounds under evaluation. The spatial arrangement is significant because it is crucialto understanding how drug molecules interact with biological receptors. The Londondispersive force, which is greatly involved in the interaction between drug molecules and receptors, is another factor that influences molar refractivity in addition to its dependence on molecular volume.

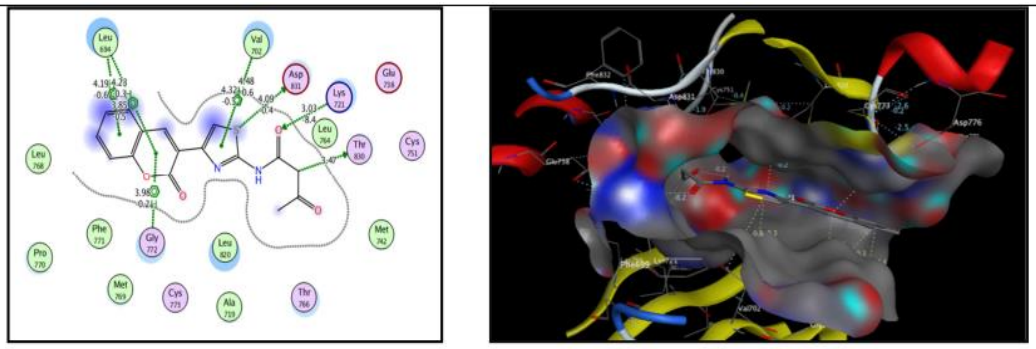

Figure (4): Binding mode of compound 3 in the active site of 1M17 along with inter acting aminoacids

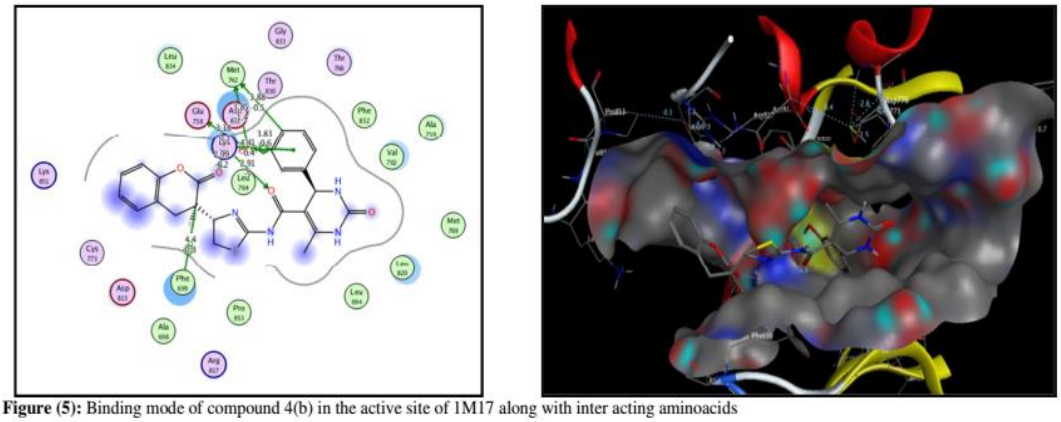

Figure (5): Binding mode of compound 4(b) in the active site of 1M17 along with inter acting aminoacids

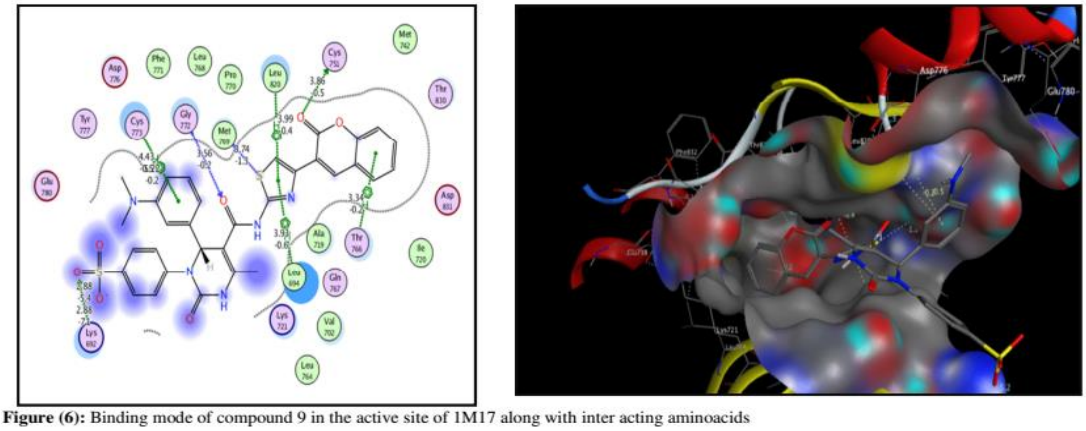

Figure (6): Binding mode of compound 9 in the active site of 1M17 along with inter acting aminoacids

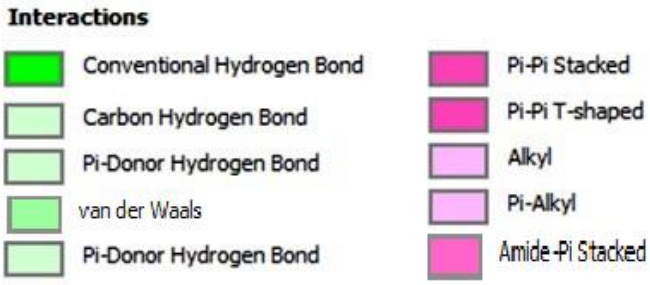

Scheme I Representative keys for the type of interactions between newly substrate synthesized Coumarin derivatives compounds **(2,3-4a,4b,8 and 9)**docked in the active site ofwith TKD**(PDB ID: 1M17)** receptor (2D and 3D ligand-receptor interactions).

According to the findings in Table 4, the size (volume) and molecular weight of proposed hybrid Coumarin derivativesare often proportional to polarizability data, molecular refractivity andsurface area grid Such as compound (**9)** which has the highest refractivity (173.83Å^3), maximum polarizability value (66.55 Å^3), surface area grid(934.22 Å^3) and has the highest molecular weight (MW) (657.72amu).On the other hand,Coumarinthiazolenucleus compound (**2)** which has lower values in all descriptors molecular volume,polarizability, refractivity, surface area grid and MW are (668.8 Å^3, 27.52Å^3, 65.45Å^3, 419.33Å^2,244.27amu), respectively. From Table 4, the other hybrid Coumarin derivativesintermediatebetween the maximum and minimum hybrid Coumarin derivatives with vary in the properties toward EGFRinhibition. Table 3 illustrates the same pattern in all descriptors ordered as **2<3<4b<4a<8<9.**

Lipophilicity is a major determinant of many ADME properties. Log P expresses the portioning of the drug molecules between aqueous medium outside the cell membrane and the lipid nature of the cell membrane This means that compounds with a lower *Log P*, are more polar and have poorer lipid bilayerpermeability, whereas compounds with a higher *Log P* are more nonpolar and poorly aqueous solubility [26,44]. For that, all compounds haveranged **1.63**to**2.18 except compound 9 equal 7.01** log P values of solubility meaning.

Furthermore, *Log P* values of compounds **4b<2<3<8<4a less than 5 and only compound (9) more than 5** of the field of optimal values (0 <*Log P*<5) [45]. It can be concluded that theseseries have a good oral bioavailability and also Coumarin derivative (**9**)have a good biological activity whichneeds a drug delivery carrier to deposit on the surface of suitable nanomaterial with specific properties to enhance oral bioavailability which is very near to optimal value range.

3.2. Density functional theory (DFT)

The obtained results in **Table 4** exhibit an increase in the values of hydrophobic, causing a decline in hydration energy. The hydration energy is determining the various molecular conformations stability in aqueous solutions [42,43]. The change in the hydration energy value is affected by the increase or decrease in the hydrogen bonds (acceptors and donors) number. Table 4 illustrates the absolute values of hydration energy ordered as with values of (-19.08, -18.62, -10.65, -10.26, -8.83 and -6.85 kcal/mol) corresponding to order **9>4b>4a>2>8>3**respectively, and characterized by hydrogen bonds (acceptors and donors) which is indicate the best potent candidates will be both **9 and 4b** compound in the interaction in biological system.

Table 4: The physico-chemical properties analysis and QSAR properties of the newly synthesized Coumarin derivatives compounds **(2,3-4a,4b,8 and 9)**towards**Epidermal Growth Factor Receptor (EGFR)** (PDB ID: 1M17)receptor for drug designing

Compounds	Polarizability (*A3*)	Refractivity (*A3*)	Vol (*A3*)	Surface area(Grid) *A2*	HE (*kcal/mol*)	Log P	MW (DA)
2	27.52	65.45	668.80	419.33	-10.26	1.92	244.27
3	35.03	83.72	881.04	454.86	-6.85	1.96	328.34
4a	55.12	137.53	1324.30	759.60	-10.65	2.18	501.56
4b	50.73	124.79	1217.62	714.00	-18.62	1.63	474.49
8	58.87	147.09	1425.71	814.01	-8.83	2.17	543.60
9	66.55	173.83	1648.51	934.22	-19.08	7.01	657.72

Values are mean ± SD duplicate assays.

3.2.1. Molecule orbital calculations

The optimized geometrical parameters (bond lengths, bond angles and dihedral angles), natural charges, natural population of the nucleus of proposed derivatives, reactivity descriptors, molecular electrostatic potential maps and energetic of the ground state for the studied Coumarins derivatives were computed and analyzed. From the elemental analysis and spectroscopic data.

3.2.2. Ground state geometry and tautomeric structures

Compound **8** and **9**can be existed in two stable configurationally isomers as a result of proton transfer from N29-amide to O39-carbonyl **H34-N29-C30-O39**, namely Amide and Imidic configurations **(Figure 7)**. We investigated the two possible isomers of the proposed compound and corresponding transition states (TS) optimized structures calculated at the B3LYP /6-311++G(d,p) level are given in Figure 1. The proposed relative potential energy surface diagram for different both tautomeric forms and TS, are represented in **(Figure 7)**. Inspection of these data reveals that the Amide configuration is the most stable one than the Imidic isomer for both derivatives **8-9** by 14.95 and 14.42 kcal/mol, and the potential barrier of TS is 44.73 and 47.0 kcal/mol respectively.

The optimized geometry, numbering system, vector of the dipole moment, bond lengths, bond angles and dihedral angles of all **Coumarin** derivatives **(2,3-4a,4b,8 and 9)**to benchmark were demonstrated in (**Figure 8)**. For the selected geometrical parameters, we have decided to compare the gas-phase B3LYP /6-311++G(d,p) estimates to the available crystal data X-ray structure of**4-(3-Coumarinyl)-3-benzyl-4-thiazolin-2-one 4-methylbenzylidenehydrazone** (**ref. CCDC**

1103657). The calculated mean absolute errors (MAEs) for selected bond lengths and angles of the Coumarin nucleus are given in (**Table 5)**. Careful inspection shows that MAEs range from 0.0 to 0.09 Å in bond length, from 0.0 to 3.21 degrees in bond angles and from 0.0 to 3.33 degrees in dihedral angles in hybrid functionals (B3LYP) which give complete reducibility in predicting bond lengths and angles with experimental results with respect to computational time and power use. Therefore, the B3LYP/6-311++G(d,p) level of theory is selected for geometry optimizations and all rest calculations in this study.In the case of compounds **(2,3-4a,4b,8 and 9)**derivatives, the majority of the calculated bond lengths show underestimation with percent ranging from 0.0 to 5.1% in C12-O15, O15-C16, C16-C21, C18-C19, C26-O27, C32-C33, C32-C37, C35-C36 and C36-C37 and overestimation with percents ranging from 1.1 to 12.6% in other bond lengths.

Generally, there is a slight change within the region of derivatives group. Inspection of the values of the dihedral angles compiled in Table 5 shows that almost all molecules are planar of thiazolecoumarinegroupand4-phenyl-3,4-dihydropyrimidin-2-onemoiety active center, which are out of plane in all the selected compounds **(4a,4b,8 and 9)**with dihedral anglesD(O39,C30,N31,C32), D(C30,N31,C32,C40) ranging from 89 to 160 degrees. The calculated values of bond angles vary between 110.0 and 124.0 degrees, which nicely compare a regular SP^3 hybridization methyl group and SP^2 hybridization in the rest of the molecule inside benzene rings, thiazole and pyrimidinonegroups geometry, respectively.

Furthermore, target molecules**(2,3,4a,4b,8 and 9)** contained C, O, N, S aromatic and non-aromatic rings with single-double resonance with bond length ranging from 1.2 to 1.75 Å and bond angle ranging from 110.0 to 125.0 degrees which is correlated to the basic concepts of hybridization of molecular orbitals. The synthesized compounds **(2,3,4a,4b,8 and 9)**are so close together in the geometrical structure planarity of the thiazolecoumarine group, with consistency in bond length, angle, and dihedral angle, but the changes are localized in the C25 derivatives group, which also nicely compares to regular sp2 and sp3 hybridization geometry, respectively.

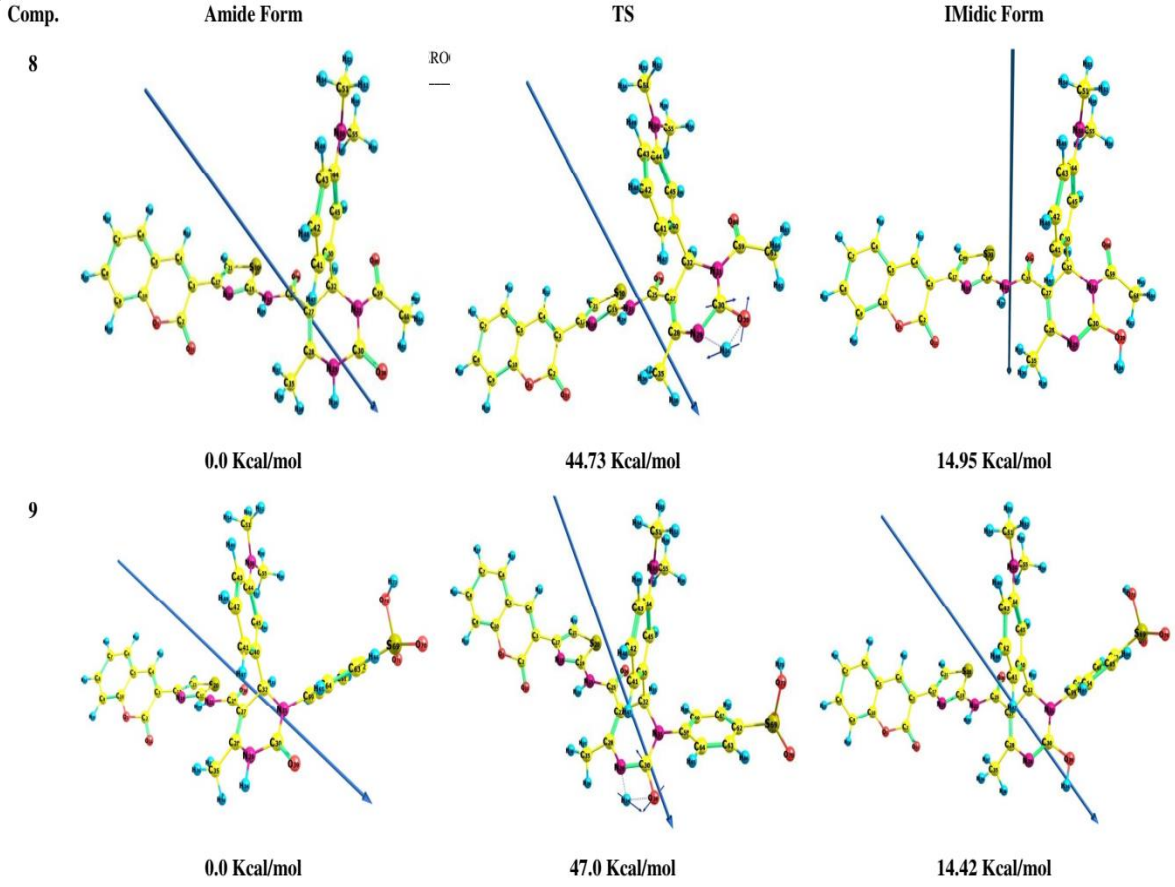

Figure 7. The optimized geometry, numbering system, vector of dipole moment, relative energy with respect to Amide form of the newly synthesized Coumarin compounds (**8 and 9)** with TS imaginary normal mode localized **H34-N29-C30-O39** using B3LYP/6-311++g(d,p) level of calculation.

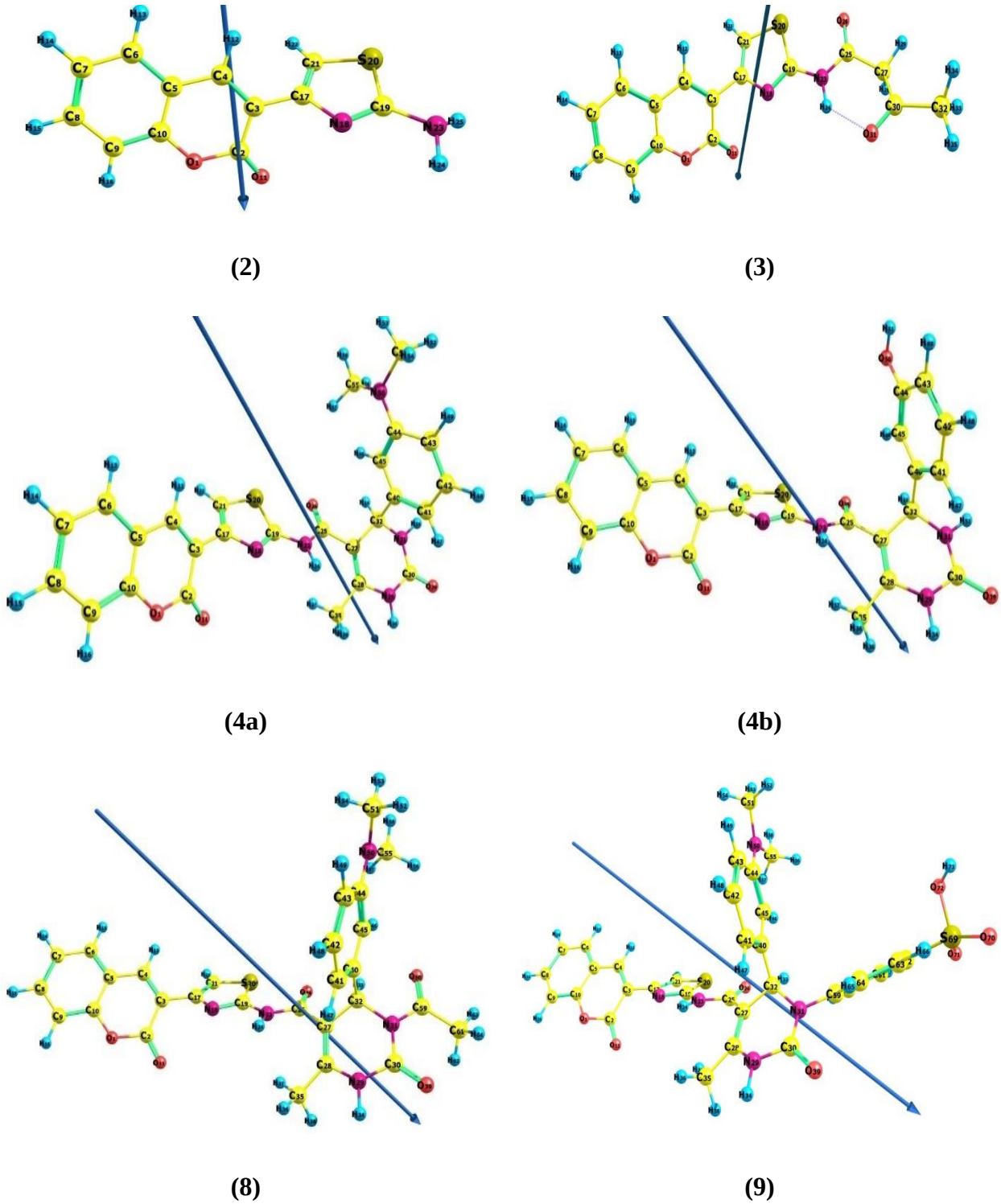

Figure 8. The optimized geometry, numbering system, vector of dipole moment of the newly synthesized Coumarin derivatives compounds**(2,3-4a,4b,8 and 9)** using B3LYP/6-311++g(d,p) level of calculation.

Table 5: The selected bond length (Ao), bond angles and dihedral angles, (degree) ofX-ray crystal structure of 4-(3-Coumarinyl)-3-benzyl-4-thiazolin-2-one 4 methylbenzylidenehydrazone(ref. CCDC 1103657)[1] and the newly synthesized Coumarin derivatives compounds (2,3-4a,4b,8 and 9) using B3LYP/6-311++g(d,p)

	exp.	**2**	**3**	**4a**	**4b**	**8**	**9**
R(O1,C2)	1.371	1.398	1.398	1.397	1.397	1.396	1.396
R(O1,C10)	1.382	1.362	1.362	1.363	1.363	1.363	1.363
R(C2,C3)	1.457	1.475	1.475	1.475	1.475	1.475	1.475
R(C2,O11)	1.211	1.199	1.199	1.200	1.200	1.200	1.200
R(C3,C4)	1.347	1.356	1.356	1.357	1.357	1.357	1.357
R(C3,C17)	1.475	1.475	1.476	1.475	1.475	1.475	1.475
R(C4,C5)	1.429	1.437	1.437	1.437	1.437	1.437	1.436
R(C5,C6)	1.400	1.407	1.407	1.407	1.407	1.407	1.407
R(C5,C10)	1.382	1.404	1.404	1.404	1.404	1.404	1.404
R(C6,C7)	1.365	1.385	1.385	1.385	1.385	1.385	1.385
R(C7,C8)	1.378	1.402	1.402	1.402	1.402	1.402	1.402
R(C8,C9)	1.381	1.389	1.389	1.389	1.389	1.389	1.389
R(C9,C10)	1.378	1.394	1.394	1.394	1.394	1.394	1.394
R(C17,N18)	1.400	1.382	1.378	1.379	1.379	1.379	1.379
R(C17,C21)	1.329	1.364	1.366	1.366	1.366	1.366	1.366
R(N18,C19)	1.368	1.295	1.298	1.298	1.298	1.298	1.298
R(C19,S20)	1.748	1.771	1.757	1.755	1.754	1.754	1.754
R(C19,N23)	1.301	1.375	1.387	1.385	1.386	1.386	1.387
R(S20,C21)	1.737	1.745	1.738	1.740	1.740	1.740	1.740
R(N23,H24)		1.011	1.020	1.010	1.010	1.010	1.010
R(N23,C25)			1.366	1.382	1.381	1.381	1.380
R(C25,O26)			1.219	1.225	1.224	1.222	1.225
R(C25,C27)			1.529	1.483	1.484	1.488	1.483
R(C27,C28)				1.353	1.353	1.347	1.350
R(C27,C32)				1.525	1.524	1.514	1.519
R(C28,N29)				1.391	1.392	1.398	1.392
R(C28,C35)				1.506	1.506	1.504	1.505
R(N29,C30)				1.399	1.399	1.389	1.400
R(C30,N31)				1.361	1.362	1.396	1.375
R(C30,O39)				1.219	1.219	1.215	1.218
R(N31,C32)				1.465	1.464	1.495	1.485
R(C32,C40)				1.532	1.533	1.531	1.530
R(C40,C41)				1.397	1.401	1.399	1.399
R(C40,C45)				1.394	1.394	1.393	1.393
R(C41,C42)				1.392	1.391	1.392	1.391
R(C42,C43)				1.390	1.394	1.390	1.391
R(C43,C44)				1.412	1.395	1.411	1.411
R(C44,C45)				1.413	1.396	1.412	1.414
R(C44,O50)					1.369		
R(C44,N50)				1.390		1.388	1.387
R(N50,C51)						1.454	1.454
R(N50,C55)				1.455		1.457	1.456
R(C59,O60)						1.214	1.399

A(C2,O1,C10)	122.48	123.54	123.52	123.56	123.56	123.57	123.59
A(O1,C2,C3)	117.55	115.97	115.98	116.01	116.01	116.00	115.99
A(O1,C2,O11)	116.63	117.37	117.42	117.37	117.35	117.34	117.38
A(C3,C2,O11)	125.81	126.64	126.59	126.62	126.64	126.65	126.62
A(C2,C3,C4)	119.61	120.04	120.05	120.00	119.98	119.98	120.00
A(C2,C3,C17)	118.09	117.95	117.91	117.93	117.97	117.97	117.95
A(C4,C3,C17)	122.08	121.99	122.02	122.05	122.03	122.03	122.02
A(C3,C4,C5)	121.77	121.94	121.93	121.96	121.97	121.97	121.98
A(C4,C5,C6)	123.97	124.01	124.00	124.01	124.01	124.02	124.02
A(C4,C5,C10)	118.08	117.47	117.47	117.47	117.48	117.47	117.46
A(C6,C5,C10)	117.95	118.51	118.52	118.50	118.50	118.50	118.50
A(C5,C6,C7)	120.38	120.55	120.54	120.53	120.53	120.53	120.53
A(C6,C7,C8)	120.14	119.84	119.83	119.85	119.85	119.85	119.85
A(C7,C8,C9)	121.20	120.75	120.76	120.76	120.76	120.76	120.76
A(C8,C9,C10)	117.83	118.98	118.98	118.96	118.96	118.96	118.96
A(O1,C10,C5)	120.46	120.89	120.91	120.87	120.86	120.86	120.86
A(O1,C10,C9)	117.05	117.74	117.73	117.74	117.74	117.74	117.74
A(C5,C10,C9)	122.48	121.37	121.36	121.39	121.40	121.40	121.40
A(C3,C17,N18)	122.85	119.98	119.94	119.97	119.99	119.98	120.07
A(C3,C17,C21)	124.48	124.14	124.84	124.89	124.91	124.92	124.84
A(N18,C17,C21)	112.67	115.88	115.21	115.14	115.09	115.10	115.08
A(C17,N18,C19)	113.63	111.18	110.80	110.77	110.74	110.73	110.76
A(N18,C19,N23)	123.13	124.00	120.90	120.58	120.49	120.52	120.48
A(C19,S20,C21)	89.85	88.11	87.65	87.61	87.59	87.58	87.60
A(C17,C21,S20)	113.20	110.05	110.75	110.78	110.82	110.81	110.81
A(C19,N23,C25)			125.27	125.85	125.84	125.83	125.84
A(N23,C25,O26)			123.04	120.50	120.67	121.07	120.72
A(N23,C25,C27)			116.49	116.84	116.88	116.23	116.93
A(O26,C25,C27)			120.42	122.63	122.42	122.68	122.31
A(C25,C27,C28)				125.34	125.46	125.47	126.14
A(C25,C27,C32)				113.77	113.71	114.58	113.77
A(C28,C27,C32)				120.78	120.68	119.84	119.96
A(C27,C28,N29)				119.22	119.17	117.61	118.13
A(C27,C28,C35)				127.66	127.62	128.72	128.29
A(N29,C28,C35)				113.10	113.18	113.63	113.55
A(C28,N29,C30)				124.70	124.61	126.02	125.12
A(N29,C30,N31)				114.06	114.02	113.83	114.38
A(N29,C30,O39)				121.15	121.22	120.38	120.16
A(N31,C30,O39)				124.76	124.73	125.78	125.43
A(C30,N31,C32)				126.17	126.02	120.19	122.51
A(C27,C32,N31)				110.05	110.07	110.82	111.25
A(C27,C32,C40)				111.55	111.57	112.93	112.06
A(N31,C32,C40)				112.91	112.79	111.96	112.42
A(C32,C40,C41)				121.40	121.35	121.63	121.53

A(C32,C40,C45)				118.45	119.00	118.37	118.34
A(C41,C40,C45)				120.14	119.65	120.01	120.12
A(C40,C41,C42)				118.83	119.79	118.97	118.80
A(C41,C42,C43)				121.47	120.76	121.39	121.50
A(C42,C43,C44)				120.61	119.36	120.59	120.63
A(C43,C44,C45)				117.32	120.23	117.40	117.24
A(C43,C44,N50)						121.57	121.60
A(C45,C44,N50)						121.02	121.16
A(C40,C45,C44)					120.21	121.63	121.69
A(C62,S69,O70)							109.20
A(O70,S69,O71)							122.54
D(C10,O1,C2,C3)	2.60	4.16	4.04	3.89	4.19	4.27	3.89
D(C10,O1,C2,O11)	-176.43	-174.79	-174.92	-175.14	-174.90	-174.82	-175.17
D(C2,O1,C10,C5)	-2.58	-1.54	-1.40	-1.52	-1.64	-1.73	-1.59
D(C2,O1,C10,C9)	176.69	178.42	178.53	178.42	178.33	178.22	178.37
D(O1,C2,C3,C17)	-175.87	177.63	177.59	178.01	177.76	177.76	178.26
D(O11,C2,C3,C17)	3.06	-3.53	-3.56	-3.05	-3.26	-3.25	-2.78
D(C4,C5,C6,C7)	179.29	-178.71	-178.72	-178.89	-178.77	-178.84	-178.94
D(C8,C9,C10,O1)	179.81	-179.82	-179.82	-179.86	-179.83	-179.79	-179.86
D(C21,C17,N18,C19)	-1.59	0.15	-0.01	-0.03	-0.02	0.00	-0.07
D(C17,N18,C19,N23)	-179.20	176.30	-179.98	-179.69	-179.34	-179.26	-179.31
D(N23,C19,S20,C21)	-179.92	-176.60	179.98	179.62	179.23	179.14	179.23
D(C19,S20,C21,C17)	-0.96	0.42	0.03	0.30	0.43	0.42	0.39
D(C19,N23,C25,O26)			-0.03	4.85	5.35	4.98	5.64
D(C19,N23,C25,C27)			-177.63	-177.34	-176.76	-176.65	-176.23
D(C28,N29,C30,O39)				-170.79	-170.02	-168.59	-163.83
D(O39,C30,N31,C32)				-167.56	-167.41	-160.28	-168.63
D(C30,N31,C32,C40)				100.17	99.36	89.10	96.05
D(C32,C40,C41,C42)				-179.04	-178.68	178.69	-179.34
D(N50,C44,C45,C40)						-178.14	-178.17
D(S69,C62,C63,C64)							178.39
D(C61,C62,S69,O70)							-159.23

3.2.1.2. Natural charges and natural population

Natural charge analysis performed on the electronic structures of target compounds **(2,3-4a,4b,8 and 9)**clearly describes the distribution of electrons in various subshells of their atomic orbitals. The charge analysis carried out for all compounds using B3LYP/6-311++G(d,p) level of calculation is presented in **(Table 6). In Table 6**, the most electronegative charges for **(2,3-4a,4b,8 and 9)** are accumulated on O70, O71, O72, N29, O39, O26, O11, O1and N18 from -0.904 e to -0.484 e.

According to an electrostatic point of view, these electronegative atoms tend to haveelectrons.However, the most electropositive atomsfor hybrid Coumarinderivatives**(2,3-4a,4b,8 and 9)**such asS69, C30, C2,C25, C10, H24 and S20for all series from +2.252e to +0.352e whichend to accept electrons active sites.Going from derivatives**2 to 9**a minor change in natural charge with the almost same pattern of sequence of the electrostatic mapping with ordering.In-depth investigation of natural charge pattern of active target hybrid Coumarin derivatives very helpful for deeper understanding of the important interaction between these active sites from compounds and biological receptors of the natural charge of hybrid Coumarin derivatives is extremely beneficial for gaining insight into the crucial interactions between title hybridCoumarin derivatives and biological receptors of Epidermal Growth Factor Receptor tyrosine kinase domainwhich enhances the investigation of cytotoxicity activity.

Table 6: Natural charge of selected atoms of the newly synthesized Coumarin derivatives compounds (2,3-4a,4b,8 and 9) Frontier molecular orbitals (FMOs)and global reactivity descriptors analysis using B3LYP/6-311++g(d,p) level of calculation.

	1	**252**	**253**	**254**		**255**		**256**		**257**
N1	-0.501	-0.502	-0.502	-0.500		-0.501		-0.502		-0.503
C2	0.829	0.829	0.819	0.829		0.830		0.829		0.818
N3	-0.638	-0.638	-0.634	-0.637		-0.637		-0.638		-0.633
C4	0.643	0.644	0.641	0.644		0.644		0.644		0.641
C5	-0.347	-0.346	-0.351	-0.342		-0.341		-0.346		-0.354
C6	0.090	0.089	0.086	0.090		0.089		0.090		0.085
O7	-0.614	-0.613	-0.630	-0.621		-0.621		-0.614		-0.632
H8	0.421	0.421	0.421	0.421		0.422		0.421		0.421
O9	-0.590	-0.589	-0.591	-0.586		-0.584		-0.589		-0.591
C12	0.300	0.300	0.327	0.303		0.302		0.300		0.298
C13	0.095	0.096	0.084	0.082		0.089		0.096		0.204
C14	0.091	0.091	0.075	0.079		0.085		0.090		0.074
C15	0.090	0.090	0.110	0.103		0.101		0.090		0.089
O16	-0.603	-0.599	-0.598	-0.595		-0.594		-0.599		-0.602
O19	-0.734	-0.733	-0.582	-0.573		-0.565		-0.733		-0.609
O21	-0.756	-0.752	-0.566	-0.566		-0.569		-0.752		-0.596
C23	-0.027	-0.039	-0.044	-0.040		-0.039		-0.037		-0.040
O26	-0.763	-0.603	-0.571	-0.572		-0.574		-0.598		-0.568
H27	0.484	0.483						0.482		
H28	0.497	0.488						0.487		
C27			0.834	0.830		0.802				0.818
C28			0.832	0.833		0.814				0.942
H29	0.475									
C29		0.825	0.825	0.824		0.825		0.801		0.800
O30		-0.579	-0.592	-0.592		-0.591		-0.589		-0.603
C31		-0.472	-0.471	-0.471		-0.472		-0.198		-0.197
C34		-0.378	-0.378	-0.377		-0.377		0.353		0.350
C37		-0.372	-0.371	-0.371		-0.371		**C35**	-0.237	-0.242
C40		-0.371	-0.371	-0.371		-0.371		**C36**	-0.133	-0.136
C43		-0.372	-0.371	-0.371		-0.371		**O41**	-0.530	-0.533
C46		-0.374	-0.374	-0.374		-0.374		**C42**	-0.207	-0.206
C49		-0.377	-0.377	-0.377		-0.377		**O46**		-0.530
C52		-0.569	-0.569	-0.569		-0.569		**C48**		-0.196
O56			-0.591	-0.597		-0.586		**C49**		-0.204
C57			-0.463	-0.464		-0.177		**C51**		-0.200
C60			-0.367	-0.367		**C58**	-0.141	**H56**		0.208
C66			-0.371	-0.372		**C59**	-0.226	**H57**		0.217
C72			-0.375	-0.378		**O68**	-0.588	**O58**		-0.617
C78			-0.306	-0.378		**C69**	-0.167	**C59**		-0.204

C81			-0.389	-0.576		**C70**	-0.141	**C60**		-0.153
O84			-0.597	-0.598		**C71**	-0.226	**C61**		-0.204
C85			-0.462	-0.462		**C73**	-0.226	**C62**		-0.175
C88			-0.373	-0.371		**C74**	-0.134	**C63**		-0.204
C91			-0.370	-0.371		**Cl77**	0.018	**C64**		-0.163

Frontier molecular orbitals (FMOs)and global reactivity descriptors analysis

The density functional theory (DFT) uses the chemical system's electron density to explain several basic ideas about how chemicals react[61].The global descriptors by framework of finite differences approximation are used to address the various qualitative concepts in chemical reactivity as cited in previous work [62-64] which calculated at B3LYP /6-311++G (d, p) level of theory. In chemistry, understanding the nature of chemical interactions and predicting the chemical reactivity of molecules, atoms, or ions are thetwo most challenging problems Frontier molecular orbitals of proposed series as present in **(Figure 9)** and results in **(Table 7) and (Table 8),** among all potential hybrid Coumarin derivatives, compound **3** displayed higher stabilityand less reactivity with an energy gap value of 4.07 eV, whereas Coumarin compound (**8**) (ΔE_g =3.14 eV) showed the lowest stability and highest reactivity [65-67].

The energy gaps of the rest of the hybrid Coumarin derivatives were ordered as follows: **4a<9<2<4b**.Due to the significance of the parameters such as I (potential ionization) and A(electronaffinity), their calculations enable us to determine the global reactivity descriptors. The Iand A parameters are related to the one-electron orbital energies of the HOMO andLUMO.The electronegativity (X) describes the tendency of an atom in the covalent bond to drawelectrons towards it. From the obtained electronegativity of the synthesized compounds Obtained results **(Table 7 and Table 8)** exhibited that compound**4b**had the highest values of I (6.28 eV) and compound **9**values of A (2.38 eV) and the electronegativity (X) (4.30, 4.03 eV, respectively).Among all, compound **3**with the highestvalue of η = 2.03 eV is the chemically hardest compound, while Coumarin derivatives **8** has the lowestvalues I (5.43 eV),X (3.86 eV) and η (1.57 eV) but compound **3** has the lowest value A (2.18), S (0.246) eV which is chemically soft and more reactive. The I and X value of the other hybrid Coumarin derivatives the same pattern order are **4b>3>2>9>4a>8.** The η value of the other hybrid Coumarin derivatives order are **3>4b>2>9>4a>8**.The A value of the other hybrid Coumarin derivatives order are **3>2>8>4a>4b>9**.In terms of globalsoftness (S), The S value of the other hybrid Coumarin derivatives perfectly opposite pattern of energy gap order are **3<4b<2<9<4a<8**. A general idea of charge transfer inanymolecule's ground state can be obtained from the electronic chemical potential V value. In terms of chemical potential, compound **8** has the greatest value (-3.86 eV), whereas **4b** has the lowest (-4.30 eV), and other hybrid Coumarin derivativeswere ordered as follows: **8>4a>9>2>3>4b(Table 7).**

Targets derivatives **(2,3-4a,4b,8 and 9)**have almost similar HOMO and LUMO isodensity dispersion on Coumarinnucleusand group attached to pyrimidine ring as depicted in Figure 9,. The direction of the electronic charge transfer motion is represented by the dipole moment vector with the order norm vector of novel synthesized Coumarincompounds are ordered as**2<3<8<4b<4a<9.**

A thermodynamic parameter that is represented by the electrophilicity index (ω) estimatesthe energy changes that occur when a chemical system reaches saturation with the addition ofmore electrons. This is very beneficial in determining a system's chemical reactivity. As shownin **(Table 7 and 8),** compound **3**nucleophilic in nature with the lowest electrophilicityindexvalue equal to 4.37 eV and **compound 8**high nucleophilic index (N) equal to -1.22 eV while compound **9** is strongly electrophilic in nature (ω =4.92 eV) and compound **4b** least nucleophilic index (N) equal to -2.07 eV. The electrophilicity shows behavior with order**9>8>4a>4b>2>3**whilenucleophilicityindexes order are **8>4a>9>2>3>4b.**

Table 7: Energetic parameters of the newly synthesized Coumarin derivatives compounds **(2,3-4a,4b,8 and 9)** using B3LYP/6-311++g(d,p) level of theory

Parameters	**ET, au**	**EHOMO, au**	**ELUMO, au**	**Eg,eV**	**μ, D**	**I,eV**	**A,eV**
2	-1120.45899	-0.22313	-0.08094	3.87	3.57	6.07	2.20
3	-1425.84945	-0.22981	-0.08027	4.07	3.89	6.25	2.18
4a	-1977.94978	-0.20326	-0.08450	3.23	7.45	5.53	2.30
4b	-1919.19314	-0.23097	-0.08479	3.98	6.42	6.28	2.31
5	-2071.84318	-0.22656	-0.08290	3.91	6.27	6.16	2.26
6	-2129.38596	-0.22273	-0.08107	3.85	4.39	6.06	2.21
7	-2055.34018	-0.20411	-0.07849	3.42	8.24	5.55	2.14
8	-2130.64103	-0.19949	-0.08427	3.14	4.88	5.43	2.29
9a	-2832.93618	-0.20871	-0.08745	3.30	11.16	5.68	2.38

Values are mean ± SD duplicate assays.

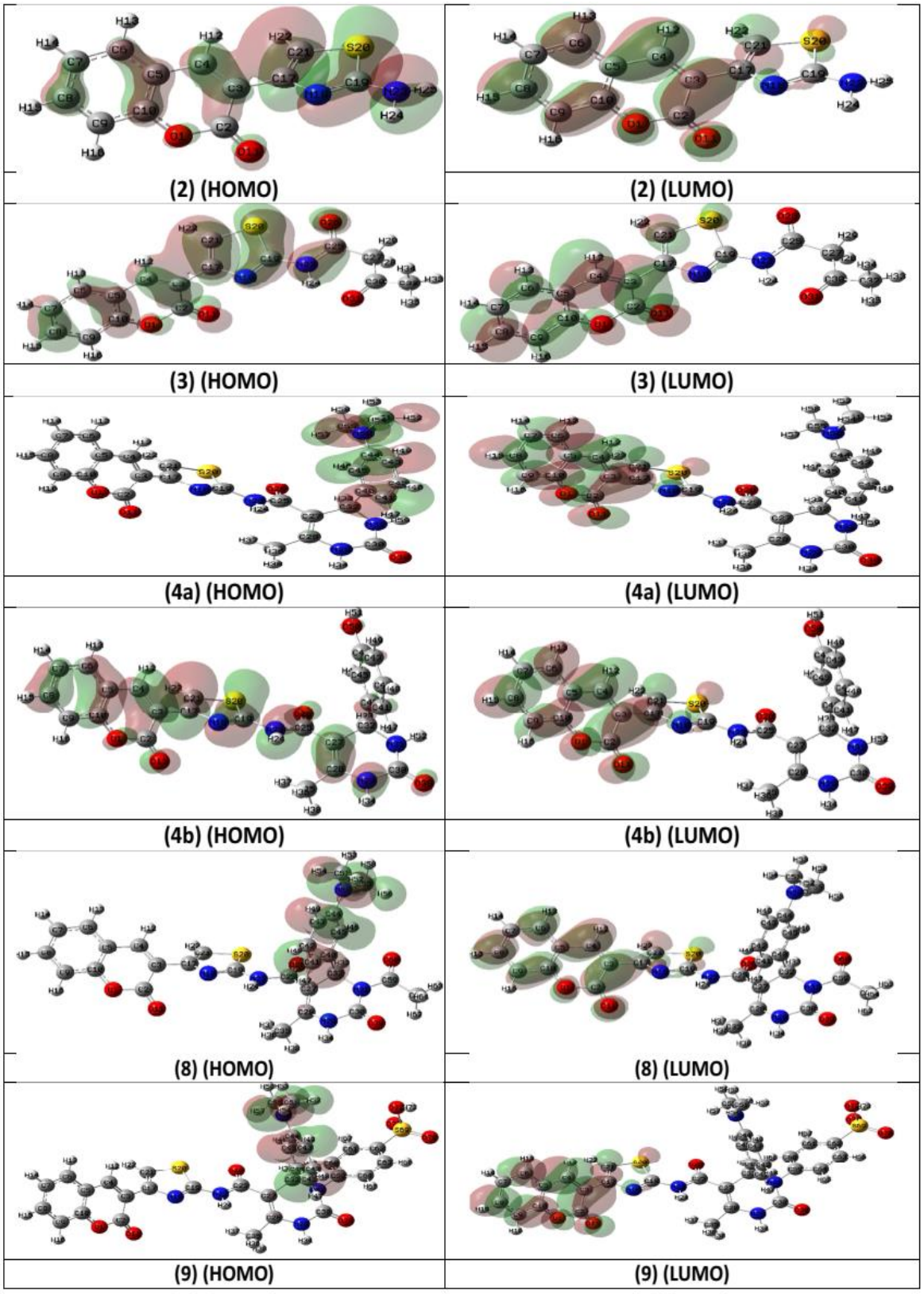

Figure 9: Frontier molecular orbitals of the newly synthesized Coumarin derivatives compounds **(2,3-4a,4b,8 and 9)** using B3LYP/6-311++g(d,p) level of calculation.

Table 8: Reactivity indices of the newly synthesized Coumarin derivatives compounds **(2,3-4a,4b,8 and 9)** using B3LYP/6-311++g(d,p) level of theory

Parameters	X,eV	η,eV	S,eV	V,eV	ω, eV	N, eV
2	4.14	1.93	0.26	-4.14	4.42	-1.86
3	4.22	2.03	0.25	-4.22	4.37	-2.04
4a	3.92	1.62	0.31	-3.92	4.74	-1.32
4b	4.30	1.99	0.25	-4.30	4.64	-2.07
5	4.21	1.95	0.26	-4.21	4.53	-1.95
6	4.13	1.93	0.26	-4.13	4.43	-1.85
7	3.84	1.71	0.29	-3.84	4.32	-1.34
8	3.86	1.57	0.32	-3.86	4.75	-1.22
9a	4.03	1.65	0.30	-4.03	4.92	-1.47

Values are mean ± SD duplicate assays.

3.2.1.4. Local reactivity descriptor:

To study site selectivity and chemical reactivity of a molecule, the principles of localreactivity descriptors have been frequently applied [11,12]. The Fukui function is a localdescriptor that can be used to study molecular site selectivity [13]. It is the first derivativeof the electronic density ρ(r) in relation to the electron numbers (N) of a system at aconstant external potential *v*(r) [53], as represented in the following equation:

$$f(r) = \left(\frac{\partial \rho(r)}{\partial N}\right)_{v(r)} = \frac{1}{2}\left(\frac{\partial \mu}{\partial v(r)}\right)_{v(r)}$$

Based on the changes in electrical density throughout a reaction process, we cancalculate Fukui functions to identify the active sites. As shown in the following equation,for the three different environments of chemicals. The Fukui functions $f^{+}(r)$, $f^{-}(r)$ and $f^{0}(r)$ are calculated for three chemical situations, using the following equations as [14–16]:

$$f^{-}(\mathrm{r}) = \mathrm{q_k(N)} - \mathrm{q_k(N-1)} \approx \rho^{\mathrm{HOMO}}(\mathrm{r}) \quad \text{For electrophilic attack}$$
$$f^{+}(\mathrm{r}) = \mathrm{q_k(N+1)} - \mathrm{q_k(N)} \approx \rho^{\mathrm{LUMO}}(\mathrm{r}) \quad \text{For nucleophilic attack}$$
$$f^{0}(\mathrm{r}) = \frac{1}{2}[\mathrm{q_k(N+1)} - \mathrm{q_k(N-1)}] \approx \frac{1}{2}[\rho^{\mathrm{HOMO}}(\mathrm{r}) + \rho^{\mathrm{LUMO}}(\mathrm{r})] \text{For Radical attack}$$

Where $\mathrm{q_k(N)}$ is the atomic population on the *kth* atom for the neutral molecule, while $\mathrm{q_k(N+1)}$ and $\mathrm{q_k(N-1)}$ are the atomic population on the *kth* atom for its anionic and cationic species, respectively. (**Table 9)**represent thedescriptors values of all compounds **(2,3-4a,4b,8 and 9)**computed at B3LYP/6-311++G (d, p) level.In addition to knowing how an atomic site in a molecule could beelectrophilic or nucleophilic, Labbe et al., [36] suggested an additional Dual descriptor($\Delta f(\mathrm{r})$) that is provided by the following equation:

$$\Delta f(\mathrm{r}) = f^{+}(\mathrm{r}) - f^{-}(\mathrm{r})$$

In Table 9. Obtained results indicate that the most electrophilic reactivity is on the Coumarin nucleus and estermoiety in derivatives**(2,3-4a,4b,8 and 9)** which is mostly found on the atoms: C17, C19, S20, C21, N23, C41-C45, N50 and C51 while the nucleophilic active site in target compounds**(2,3-4a,4b,8 and 9)**distributed on the Coumarin skeleton localized on O1, C2, C3, C4, C8, C9, C10 and O9.Also,when considering the Dual descriptor $\Delta f(\mathrm{r})$ for the nucleophilic and electrophilic attacks, as well as the philicity indices, the same result could be obtained. The high electronegativity of atom oxygen and nitrogen led to an electron density redistribution, in addition to the effect of para derivatives insertion of pyrimidine derivatives. These findings agree with the analysis of the natural population using calculated HOMO and LUMO.

In 2004, Chattaraj et al. proposed the generalized philicity concept; with the help of correspondingcondensed-to-atom Fukui function variations, they developed a local quantity known asphilicity coupled with a site k in a molecule (f_k^{α}), as given in the following equation [68]

$$\omega_k^{\alpha} = \omega f_k^{\alpha}$$

Where α = +, − and 0 corresponds to local philic quantities describing nucleophilic, electrophilic and radical attacks, respectively. According to the mentioned equation, the mostelectrophilic property has the highest value of ω_k^{α}. Moreover, different local softness wasproposed by Lee et al., to define the reactivity of a molecule[69] as in the followingequation.

$$s_k^{\alpha} = s f_k^{\alpha}$$

In the equation, α is represented by local softness quantities fornucleophilic (α = +), electrophilic (α = -) and radical attacks (α = 0). In order to completethe picture, the software package Multiwfn (v. 3.7) determined the local electrophilicityand nucleophilicity index, condensed local softness, and relativeelectrophilicity/nucleophilicity for each atom in the compounds from a CDFT point ofview[37]. a close inspection would show that all the compounds had the electron donating andthe back-donation processes at the center of their active sites, in agreement with the Fukuifunctions and also with the frontier orbital, as shown in the results obtained, which areboldly given in Tables 9 and 10. These findings showed the studied compounds to haveseveral active sites especially over Coumarin skeleton, thiazole linker and group attached pyrimidine derivatives which making them able to interact with the surface of pocket proteins viadonating and back donating electrons active centers. Lastly, the aforementioned local descriptors show that theexperimental cytotoxicity of caner results in this study are in agreement with the theoretical variation of thecompounds efficiency.

Table 9: Values of the relative Condensed local Softnesses (Hartree*e)ofCumarine derivatives compounds**(2,3-4a,4b,8 and 9)** using B3LYP/6-311++g(d,p) level of theory from CDFT point of view.

	2			3			4a			4b			8			9		
Atoms	**f(-)**	**f(+)**	**Δf**	**f(-)**	**f(+)**	**Δf**	**f(-)**	**f(+)**	**Δf**	**f(-)**	**f(+)**	**Δf**	**f(-)**	**f(+)**	**Δf**	**f(-)**	**f(+)**	**Δf**
O1	0.005	**0.033**	**0.029**	0.009	**0.034**	**0.024**	0.000	**0.034**	**0.034**	0.006	**0.034**	**0.027**	0.000	**0.034**	**0.034**	0.000	**0.034**	**0.034**
C2	0.012	**0.066**	**0.053**	0.015	**0.066**	**0.051**	0.000	**0.066**	**0.066**	0.012	**0.065**	**0.053**	0.000	**0.066**	**0.066**	0.000	**0.065**	**0.065**
C3	-0.004	**0.184**	**0.188**	0.036	**0.185**	**0.149**	0.000	**0.184**	**0.184**	0.029	**0.183**	**0.154**	0.000	**0.183**	**0.183**	0.000	**0.183**	**0.183**
C4	0.053	**0.242**	**0.189**	0.066	**0.244**	**0.178**	0.000	**0.247**	**0.247**	0.056	**0.247**	**0.191**	0.000	**0.247**	**0.247**	0.000	**0.249**	**0.249**
C7	0.006	0.004	-0.002	0.017	0.004	-0.012	0.000	0.004	0.004	0.011	0.004	-0.007	0.000	0.004	0.004	0.000	0.004	0.004
C8	0.023	**0.125**	**0.102**	0.041	**0.125**	**0.084**	0.000	**0.124**	**0.124**	0.033	**0.123**	**0.091**	0.000	**0.123**	**0.123**	0.000	**0.123**	**0.123**
C9	-0.001	**0.036**	**0.037**	-0.001	**0.036**	**0.037**	0.000	**0.035**	**0.035**	0.000	**0.035**	**0.034**	0.000	**0.035**	**0.035**	0.000	**0.034**	**0.034**
C10	0.019	**0.060**	**0.041**	0.036	**0.060**	**0.024**	0.000	**0.061**	**0.061**	0.027	**0.060**	**0.033**	0.000	**0.060**	**0.060**	0.000	**0.061**	**0.061**
O11	0.014	**0.055**	**0.041**	0.031	**0.055**	**0.024**	0.000	**0.055**	**0.055**	0.023	**0.055**	**0.032**	0.000	**0.055**	**0.055**	0.000	**0.054**	**0.054**
C17	**0.126**	0.003	**-0.124**	**0.110**	0.004	**-0.105**	0.001	0.004	0.003	0.099	0.003	-0.096	0.000	0.003	0.003	0.001	0.004	0.003
N18	0.057	0.005	-0.052	0.022	0.004	-0.018	0.000	0.004	0.004	0.024	0.004	-0.020	0.000	0.004	0.004	0.000	0.004	0.004
C19	**0.100**	0.002	**-0.098**	**0.108**	0.002	**-0.107**	0.003	0.002	-0.002	**0.090**	0.002	**-0.088**	-0.001	0.002	0.003	0.002	0.001	-0.001
S20	**0.111**	0.015	**-0.096**	**0.092**	0.014	**-0.079**	0.000	0.014	0.014	**0.085**	0.015	**-0.070**	0.000	0.015	0.015	0.000	0.015	0.015
C21	**0.266**	0.040	**-0.227**	**0.234**	0.035	**-0.199**	0.000	0.039	0.039	**0.209**	0.042	**-0.167**	0.000	0.042	0.042	0.000	0.042	0.042
N23	**0.170**	0.000	**-0.169**	**0.075**	0.000	**-0.075**	0.000	0.000	0.000	**0.081**	0.000	**-0.080**	0.000	0.000	0.001	0.000	0.000	0.001
C25				0.016	0.000	-0.016	-0.003	0.002	0.005	0.008	0.001	-0.007	0.000	0.000	0.000	-0.001	0.001	0.002
O26				0.033	0.000	-0.033	0.001	0.000		0.012	0.000		0.000	0.000		0.001	0.000	
C27				0.001	0.000	-0.001	0.008	-0.003		0.043	-0.002		0.004	-0.001		0.001	-0.001	
C28							-0.009	0.001	0.010	0.033	0.001	-0.032	0.005	0.000	-0.004	-0.001	0.000	0.001
N29							0.001	0.000	-0.001	0.033	0.000	-0.033	0.003	0.000	-0.003	0.001	0.000	-0.001
C30				0.001	0.000		0.001	0.000		0.002	0.000		-0.002	0.000		0.004	0.000	
O31				0.000	0.000	0.000												
N31							0.004	0.000	-0.004	0.001	0.000	-0.001	0.002	0.000	-0.002	0.007	0.000	-0.007
C32				0.000	0.000	0.000	0.009	0.001	-0.009	0.003	0.001	-0.002	0.001	0.000	-0.002	0.000	0.000	0.000
C35							0.000	0.000	0.000	0.001	0.000	-0.001	0.000	0.000	0.000	0.003	0.000	-0.003
H37							0.000	0.000	0.000	0.000	0.000	0.000	0.000	0.000	0.000	0.000	0.000	0.000
O39							0.002	0.000	-0.002	0.008	0.000	-0.008	0.001	0.000	-0.001	0.001	0.000	-0.001
C40							0.012	0.000	-0.012	0.001	-0.001	-0.002	0.007	0.000	-0.007	0.013	0.000	-0.013
C41							**0.193**	0.000	**-0.193**	0.002	0.000	-0.002	**0.188**	0.000	**-0.188**	**0.196**	0.000	**-0.196**
C42							**0.019**	0.000	**-0.019**	0.003	0.000	-0.003	0.020	0.000	-0.020	**0.013**	0.000	**-0.013**
C43							**0.126**	0.000	**-0.126**	0.004	0.000	-0.004	**0.122**	0.000	**-0.122**	**0.131**	0.000	**-0.131**
C44							**0.078**	0.000	**-0.078**	0.004	0.000	-0.003	**0.069**	0.000	**-0.069**	**0.069**	0.000	**-0.069**
C45							**0.111**	-0.001	**-0.112**	0.003	0.000	-0.003	**0.116**	0.000	**-0.116**	**0.111**	-0.001	**-0.112**
O50										0.002	0.000	-0.002						
N50							**0.336**	0.000	**-0.336**				**0.343**	0.000	**-0.343**	**0.338**	0.000	**-0.338**
C51							**0.011**	0.000	**-0.011**				0.010	0.000	-0.010	0.013	0.000	-0.013
C59													0.001	0.000	-0.001	-0.001	0.000	0.001
C60													0.001	0.000	-0.001	0.001	0.000	-0.001
C61													0.000	0.000	0.000	0.002	0.000	-0.002
C63																-0.004	0.000	0.004
C64																-0.002	0.000	0.002
S69																0.000	0.000	0.000
O70																0.000	0.000	0.000

Table 10: Values of Condensed local electrophilicity (ElP) and nucleophilicity (NuP) index (e*eV) of Coumarin derivatives compounds (2,3-4a,4b,8 and 9)using B3LYP/6-311++g(d,p) level of theory from CDFT point of view

	2		3		4a		4b		8		9	
Atoms	s+/s-	s-/s+	s+/s-	s-/s+	s+/s-	s-/s+	s+/s-	s-/s+	s+/s-	s-/s+	s+/s-	s-/s+
O1	0.710	1.410	0.889	1.125	0.362	2.763	0.589	1.699	0.373	2.684	0.441	2.269
C2	0.348	2.874	0.472	2.117	0.154	6.483	0.298	3.354	0.165	6.067	0.199	5.023
C3	0.263	3.800	0.430	2.327	0.087	11.490	0.237	4.216	0.111	8.980	0.133	7.508
C4	0.370	2.700	0.483	2.073	0.181	5.535	0.344	2.910	0.200	5.009	0.227	4.413
C7	0.967	1.034	1.212	0.825	0.492	2.031	0.813	1.230	0.521	1.921	0.613	1.632
C8	0.673	1.486	0.851	1.176	0.363	2.753	0.597	1.674	0.383	2.609	0.450	2.221
C9	0.510	1.961	0.644	1.552	0.289	3.467	0.456	2.196	0.299	3.347	0.356	2.807
C10	1.016	0.985	1.362	0.734	0.484	2.064	0.867	1.154	0.520	1.924	0.613	1.632
O11	0.595	1.682	0.843	1.187	0.261	3.833	0.501	1.996	0.282	3.541	0.340	2.940
C17	54.256	0.018	-119.717	-0.008	4.940	0.202	8.411	0.119	3.974	0.252	8.480	0.118
N18	-47.097	-0.021	-50.927	-0.020	2.842	0.352	4.566	0.219	1.716	0.583	5.520	0.181
C19	2.075	0.482	3.628	0.276	0.394	2.539	1.369	0.730	0.456	2.195	0.666	1.502
S20	1.599	0.626	1.929	0.519	0.453	2.209	1.075	0.930	0.518	1.930	0.667	1.499
C21	2.836	0.353	3.436	0.291	0.841	1.189	1.585	0.631	0.831	1.203	1.158	0.864
N23	3.836	0.261	14.008	0.071	1.262	0.792	3.502	0.286	0.796	1.256	1.794	0.558
C25			2.398	0.417	-0.018	-56.336	0.321	3.119	-0.035	-28.659	-0.016	-64.651
O26			1.888	0.530	0.200	5.000	0.730	1.370	0.261	3.832	0.386	2.594
C27			0.578	1.730	0.332	3.011	2.822	0.354	-0.072	-13.920	0.160	6.248
C28					0.665	1.503	0.975	1.025	0.474	2.111	1.003	0.997
N29					1.250	0.800	2.986	0.335	0.959	1.042	1.106	0.905
C30			0.090	11.100	0.630	1.589	0.865	1.156	0.163	6.143	0.269	3.717
O31			0.048	20.832								
N31					0.421	2.378	0.918	1.090	-0.748	-1.338	-0.715	-1.400
C32			0.451	2.218	0.954	1.048	1.192	0.839	0.566	1.768	1.380	0.724
C35					1.182	0.846	1.205	0.830	0.862	1.161	1.372	0.729
H37					-5.187	-0.193	-14.622	-0.068	8.002	0.125	21.576	0.046
O39					1.184	0.845	1.421	0.704	0.722	1.385	1.187	0.842
C40					-6.405	-0.156	-8.067	-0.124	-4.559	-0.219	-3.799	-0.263
C41					103.636	0.010	12.344	0.081	-16.298	-0.061	-30.832	-0.032
C42					4.451	0.225	1.982	0.505	5.925	0.169	5.602	0.179
C43					6.101	0.164	2.460	0.407	4.858	0.206	6.828	0.147
C44					14.876	0.067	5.391	0.186	5.227	0.191	11.604	0.086
C45					-15.067	-0.066	6.995	0.143	27.998	0.036	-11.379	-0.088
N50					2106.316	0.001			31.379	0.032	54.706	0.018
O50							7.400	0.135				

C55					26.793	0.037			10.492	0.095	19.440	0.051
C59					0.718	1.392			0.292	3.424	-0.423	-2.365
C60									0.026	38.336	-0.143	-7.017
C61									0.973	1.028	0.267	3.741
C64									0.709	1.411	-0.261	-3.839
S69											0.234	4.278
O70											0.572	1.749
H73											0.205	4.869

	2		**3**		**4a**		**4b**		**8**		**9**	
Atoms	EIP	NUP	EIP	NUP	EIP	NUP	EIP	NUP	EIP	NUP	EIP	NUP
O1	-0.032	-0.111	-0.033	-0.083	-0.013	-0.104	-0.022	-0.079	-0.012	-0.096	-0.015	-0.083
C2	-0.020	-0.146	-0.023	-0.109	-0.007	-0.132	-0.014	-0.100	-0.007	-0.121	-0.008	-0.105
C3	-0.025	-0.240	-0.033	-0.173	-0.006	-0.205	-0.017	-0.155	-0.007	-0.184	-0.009	-0.163
C4	-0.043	-0.289	-0.046	-0.214	-0.017	-0.262	-0.032	-0.199	-0.017	-0.240	-0.019	-0.209
C7	-0.048	-0.124	-0.052	-0.095	-0.020	-0.118	-0.034	-0.090	-0.020	-0.110	-0.023	-0.093
C8	-0.064	-0.236	-0.068	-0.178	-0.028	-0.220	-0.047	-0.168	-0.027	-0.204	-0.032	-0.174
C9	-0.028	-0.139	-0.030	-0.104	-0.013	-0.128	-0.021	-0.097	-0.012	-0.118	-0.014	-0.100
C10	-0.036	-0.087	-0.039	-0.064	-0.014	-0.080	-0.025	-0.061	-0.013	-0.073	-0.016	-0.063
O11	-0.061	-0.257	-0.070	-0.186	-0.021	-0.226	-0.040	-0.171	-0.020	-0.205	-0.025	-0.178
C17	-0.065	-0.003	-0.063	0.001	-0.023	-0.013	-0.045	-0.011	-0.021	-0.016	-0.026	-0.007
N18	-0.048	0.003	-0.036	0.002	-0.014	-0.014	-0.026	-0.012	-0.011	-0.019	-0.015	-0.007
C19	-0.051	-0.061	-0.053	-0.033	-0.009	-0.063	-0.029	-0.046	-0.008	-0.053	-0.011	-0.041
S20	-0.171	-0.266	-0.146	-0.169	-0.041	-0.256	-0.099	-0.197	-0.043	-0.239	-0.048	-0.178
C21	-0.113	-0.099	-0.106	-0.069	-0.038	-0.128	-0.074	-0.099	-0.036	-0.124	-0.042	-0.089
N23	-0.096	-0.062	-0.046	-0.007	-0.010	-0.022	-0.028	-0.017	-0.007	-0.025	-0.011	-0.014
C25			-0.029	-0.027	0.001	-0.083	-0.009	-0.062	0.001	-0.087	0.000	-0.040
O26			-0.054	-0.064	-0.007	-0.103	-0.027	-0.080	-0.010	-0.113	-0.008	-0.054
C27			-0.009	-0.036	-0.003	-0.027	-0.033	-0.025	0.001	-0.046	-0.001	-0.018
C28					-0.020	-0.085	-0.033	-0.072	-0.016	-0.097	-0.019	-0.047
N29					-0.014	-0.031	-0.035	-0.025	-0.009	-0.027	-0.011	-0.023
C30			-0.006	-0.152	-0.008	-0.036	-0.013	-0.032	-0.004	-0.067	-0.004	-0.039
O31			-0.003	-0.133								
N31					-0.003	-0.017	-0.006	-0.014	0.002	-0.006	0.002	-0.006
C32			-0.009	-0.045	-0.003	-0.010	-0.005	-0.009	-0.002	-0.008	-0.002	-0.003
C35					-0.008	-0.019	-0.009	-0.017	-0.007	-0.024	-0.008	-0.014
H37					-0.005	0.003	-0.004	0.001	-0.005	-0.002	-0.005	-0.001
O39					-0.038	-0.093	-0.052	-0.079	-0.029	-0.115	-0.034	-0.071
C40					-0.027	0.012	-0.009	0.002	-0.028	0.018	-0.030	0.020
C41					-0.082	-0.002	-0.038	-0.007	-0.084	0.015	-0.090	0.007
C42					-0.038	-0.024	-0.025	-0.027	-0.039	-0.019	-0.040	-0.018
C43					-0.058	-0.027	-0.038	-0.033	-0.058	-0.034	-0.063	-0.023
C44					-0.029	-0.006	-0.030	-0.012	-0.030	-0.017	-0.031	-0.007

C45					-0.040	0.008	-0.013	-0.004	-0.047	-0.005	-0.044	0.009
N50					-0.105	0.000			-0.116	-0.011	-0.115	-0.005
O50							-0.041	-0.012				
C55					-0.025	-0.003			-0.028	-0.008	-0.028	-0.004
C59					-0.009	-0.034			-0.004	-0.039	0.013	-0.076
C60									-0.001	-0.061	0.003	-0.049
C61									-0.007	-0.020	-0.007	-0.062
C64									-0.006	-0.023	0.005	-0.048
S69											-0.006	-0.061
O70											-0.015	-0.063
H73											-0.003	-0.030

3.2.1.5. Molecular electrostatic potential (MEP)

In several fields of chemistry, the electrostatic potential (ESP) on molecular surfaces has become one of the most effective tools for identifying, analyzing, and understanding trends [70,71]. It is related to electronic density, which is an excellent descriptor for describing the charge distributions on a molecule, identifying regions that are differently charged, and identifying the sites where hydrogen-bonding interactions, electrophilic properties and nucleophilic properties are most likely to take place [72]. Electrostatic potentials (ESPs) are essential for predicting and understanding intermolecular interactions [57]. The crucial interactions between the synthesized hybrids and biological targets must be better understood with the help of in-depth analysis their ESPs. The ESP as denoted by $V(r)$ (in a.u.) at a given point r (x,y,z) in the molecule's vicinity is a calculation of the electrostatic energy that a positive unit test charge would experience at that point. Negative and positive ESPs corresponded to the attractive and repulsion interactions, respectively. The following equation defines the ESP as the interaction energy between a proton at *r* and the electrical charge produced by the electrons and nuclei.

$$V(r) = \sum_{A}^{nuclei} \frac{Z_A}{|R_A - r|} - \int \frac{\rho(r')}{|r - r'|} dr'$$

Where$\boldsymbol{Z_A}$and $\boldsymbol{R_A}$are the charge and position of nucleus A, respectively, and ρ (**r'**) is the electron density at position **r'**, all in atomic units.

The Electrostatic potentials-mapped surfaces of the studiedCoumarin derivatives compounds**(2,3-4a,4b,8 and 9)**are presentedin **(Figure 10).**The overall vanderWaals surface can be divided into several fragments bythe quantitative molecular surface analysis module of the Multiwfn package, and thiscapability enables us to analyze the features of the ESP distribution.

For **ThiazoleCoumarin nucleus (2)**, the surface exhibits large negative value of ESP around the carbonyl group of Coumarin nucleusC2=O11 and nitrogen of thiazole C17-N=C19(-43.71, -45.65 kcal/mol) and three sulphurofthiazolemoiety -S20- (-7.2, -5.5 and -1.75 kcal/mol) and negative distribution on fused benzeneof coumarine(--6.9, -6.5, -6.4, -6.9kcal/mol) in specific sequence groups of the target compounds with the electron donating ability of □-carbonyl amide group attached with thethiazole increases the global minima in compound (**3)** rather than other derivatives, as (-44.68, -46.66, -6.26, -4.51, -0.24, -7.26, -7.35, -6.8, -6.9 kcal/mol) with increase of di-carbonyl (-34.16, -27.32 kcal/mol), **(Figure 10).**In other derivatives **(4a,4b,8 and 9)**,the negativity charge decreased by inject 4-phenyl-3,4-dihydropyrimidin-2-one derivatives groups with decrease electron density to overall skeleton of Coumarinthiazolederivatives which decrease negative charge differences by -3.0 to -6.8kcal/mol for different substitution by N,N dimethyl or hydroxyl group with high effect for direct meta position of phenyl than others as shown in informative (**Figure 10)**.

The global maxima of ESPs on the ThiazoleCoumarin hybrid derivatives **(2,3-4a,4b,8 and 9)**surfaces are located on the carbon with the proton of these derivatives, which vary as the same pervious pattern derivatives in case **3** rather than other derivatives **(4a,4b,8 and 9)** by **+ 0.3** kcal/molmeanwhile in case other derivative **(Figure 10)**increase the positive charge over Skelton by **+ 2.0** kcal/mole.This indicates that electrostatic or hydrogen bonding will be the main interaction between hybrid Coumarin derivatives and their target receptors with **Epidermal Growth Factor Receptor (EGFR)**(PDB ID: 1M17),The ability to generate hydrogen bond interaction and intramolecular charge transfer (ICT) via the most reactive centers, is confirmed by a careful examination of these ESP values, indicating that they can act as therapeutics. These values show the same findings and pattern from the analyses of the NBO population and local reactivity descriptors reported in the previous sections.

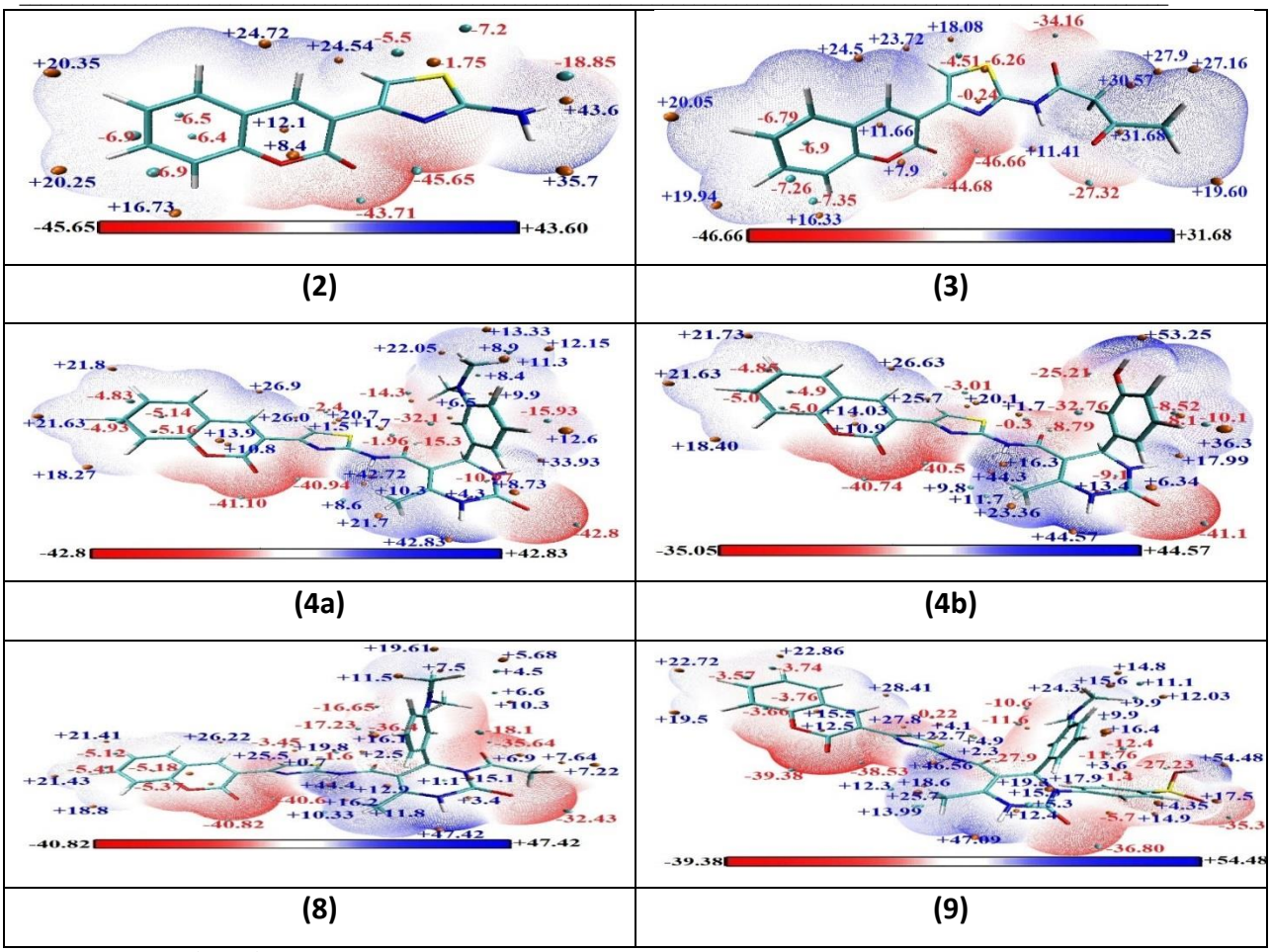

Figure 10: MEP surfaces of the newly synthesized Coumarin derivatives compounds **(2,3-4a,4b,8 and 9)** using B3LYP/6-311++g(d,p) level of calculation.

3.1. Molecular docking

(Table 3 Figure 4,5,6, and scheme I)present the proposed molecular docking scores and binding mode with representation keys for the type of interaction docking in the active site of **EGFR** (PDB ID: 1M17)[2]proteins of newly synthesized selected Coumarin derivatives series of interest **(2,3-4a,4b,8 and 9) to** predicting binding sites and binding energies with amino acids of receptor, Careful inspection of these results, Compounds derivatives indicated compound **9 and 4b** can be as good candidates for **EGFR** inhibitors agents, which is also correlated with experimental results. We will be focusing on compound **4b and 9** on next discussion of structural and conformationalstability complexes by molecular dynamics simulation over long-range MD simulation of 100 nswith free energy calculation.

Figure 4,5,6. The proposed binding mode of newly synthesized Coumarin derivatives compounds **(2,3-4a,4b,8 and 9)** docked in the active site of with tyrosine kinase domain **(TKD**) **(PDB ID: 1M17)** receptor (2D and 3D ligand-receptor interactions).

Scheme 1-4. Representative keys for the type of interactions between newly substrate synthesized Coumarin derivatives compounds **(2,3-4a,4b,8 and 9)** docked in the active site of with TKD **(PDB ID: 1M17)** receptor (2D and 3D ligand-receptor interactions).

3.2. Molecular dynamics simulation and system stability

The molecular interactions and the water solvent conditions around the protein influence the conformational stability of the protein–ligand interaction. The bestdocked structured of all series of interest (**2,3-4a,4b,8 and 9**) with **Epidermal Growth Factor Receptor (EGFR)**(PDB ID: 1M17)[2], where the best docked compounds**4b and 9**ligandsbinding with **1M17** complex which pose with the highest binding affinity was utilized as the starting structures. as well as, its interaction and stability, were predicted using a molecular dynamic simulation [73,74]. Therefore, a long-range MD simulation of 100 ns was performed on docked complexes, in order to investigate the dynamics, conformational stability, and structural stability of protein–ligand complex.

The stability of the systems was measured in this study using the Root-Mean-Square Deviation (RMSD) during the 100 ns simulations.The most acceptable RMSD value range was <5.0 Å, as the lower RMSD value indicates superior stability of the system[75,76]. For all frames of the (**1M17)**protein, ligands**(4b or 9)** andligand-protein complexes systems as presented in **(Figure 11),** the average RMSD values were6.622, 1.663 and 6.490 Å, in case **1M17-4b** complex, meanwhile in **1M17-9** complex 4.918, 1.280 and 4.918 Å, respectively. The stander deviation of the average RMSD values were 0.76, 0.52 and 0.75 Å, in case **1M17-4b** complex, meanwhile in **1M17-9** complex 0.95, 0.22 and 0.94 Å, respectively.The Average RMSD during

the 100 ns simulations verses the frame of 0.1 (ns) time ago is also analysis, as presented in **(Figure 12)** which give values were 1.234, 0.719 and 1.239 Å in case **1M17-4b** while in case **1M17-9** were 1.006, 0.636 and 0.920, respectively. The stander deviation of the average RMSD values were 0.14, 0.31 and 0.13 Å, in case **1M17-4b** complex, meanwhile in **1M17-9** complex 0.11, 0.19 and 0.09 Å, respectively.These results revealed that both system complexes stable with the **1M17-9** complex system acquired a relatively more stable conformation than the other **1M17-4b** complex studied system.

Examining residue behavior and its relationship with the ligand during MD simulation production requires evaluating protein structural flexibility upon ligand binding[75-77]. Using the Root-Mean-Square Fluctuation (RMSF) method,protein residue variations were assessed to determine the impact of inhibitor binding to the relevant targets across 100 ns of simulations. The calculated average RMSF values for the **1M17-4b** and **1M17-9** complexes to protein systems were 2.775 and 2.185 Å, respectively. The stander deviation of the average RMSF values were2.70, 1.82 Å, respectively, (**Figure 13)**depicts the overall residue fluctuations of several systems **1M17-4b** and **1M17-9**complexes. The terminal residues in contrast to the core residues were found to have more fluctuations, which are expected due to the flexible nature of the biomolecule terminals. Overall, the average RMSF of the systems is <3 Å, which indicates formation of highly stable complexes and good affinity of the ligand molecule for the receptors, which will be reflect well on the complex stability with **1M17-9** more stable than the other **1M17-4b**.

The number of hydrogen bond interactions occurred between protein and ligands were calculated with Angle cut = 10 degree, rcut = 3.0Å and plotted against time 100 ns as shown in Figure 12, Upon calculation of hydrogen bonds, the average number of hydrogen bonds per timeframe was observed to be 2.090 and 2.644 Åfor**1M17-4b** and **1M17-9 complexes,** respectively as presented in Figure 14. During overall analysis, it was found that ligand–protein interaction significantly increased the number of hydrogen bonds from 1 to 7 HBs per trajectory analysis in case **1M17-4b**complex and from 1 to 8 in case of **1M17-9** complex. These values demonstrate that the system **1M17-9** acquired a relatively more stable conformation than the other system **1M17-4b** studied by hydrogen bond forms interaction.The protein structural compactness and simulation stability are both indicated by the radius of gyration (R_g) as presented in Figure 15. For all frames of the TKD protein (**1M17**), ligands (**4b or 9**) and ligand protein complex systems, the average R_g values were2.089, 0.506 and 2.082 nm, in case **1M17-4b**, meanwhile in **1M17-9**2.016, 0.565 and 2.005 Å, respectively. The stander deviation of the average RMSD values were 0.034, 0.010 and 0.034nm, in case **1M17-4b** complex, meanwhile **1M17-9** complex were 0.032, 0.015 and 0.032.Overall, the average R_g of both protein complexes indicates compact formation of highly stable complexes with **1M17-9** will be reflect well on complex stabilities more than the other **1M17-4b** complex.

The solvent accessible surface area (SASA) of the protein was calculated during MD simulation in ligand-bound conditions due to binding of ligand to the protein. For all frames of both protein receptor (**1M17)**, ligand **(4b or 9)** and ligand-protein complex systems as presented, the average SASA valueswere173.564, 7.326 and 173.718 nm^2, in case **1M17-4b**complex, meanwhile in **1M17-9**complex 177.279, 9.470 and 175.147 nm^2, respectively.The stander deviation of the average SASA values were 4.745, 0.232 and 4.805 nm^2, in case **1M17-4b**complex, meanwhile in **1M17-9**complex 3.471, 0.279 and 3.272 nm^2, respectively. The analysis indicates the folding states of protein and its stability upon ligand binding affinity which is obvious because of the heavy nature of the complex as findings in results with slightly change in protein and its complexes.**(Figure 16)**

Figure 17shows that average distance of center of mass of protein residues (**1M17**) and ligands (**4b or 9**) throughout the 100 ns simulation. Complex**1M17-4b** show less distance compared with complex **1M17-9** are kept stay close about 1.3601, 1.1936 nm respectively as a function of time which reflect to the conformation, motion and stability of **1M17-4b**complex over the other one.

To estimate the binding between the pocket protein residues (**1M17**) and ligands (**4b or 9**) complexes, a contact frequency(CF) analysis was performed utilizing the contact Freq.tcl module on VMD and with a cut off of 4 Å as represents in Figure 18. In the simulation **1M17-4b** case study, the following amino acid residues exhibited higher CF values to 91.65%: LEU-694, GLY-695, SER-696, GLY-697, VAL-702, ALA-719, LYS-721, GLN-767, LEU-768, MET-769, GLY-772, LEU-820, THR-830. In **1M17-9** there are a good contact surfaces with the protein pocket through simulation study, the following amino acid residues exhibited higher CF values to 100.0%:GLY-695, SER-696, GLY-697, PHE-699, GLY-700, VAL-702, ALA-719, LYS-721, GLU-738, MET-742, LEU-764, THR-766, GLN-767, CYS-773, ARG-817, LEU-820, THR-830, which indicate excellent binding affinity towards Epidermal Growth Factor Receptor (EGFR) inhibition complex.

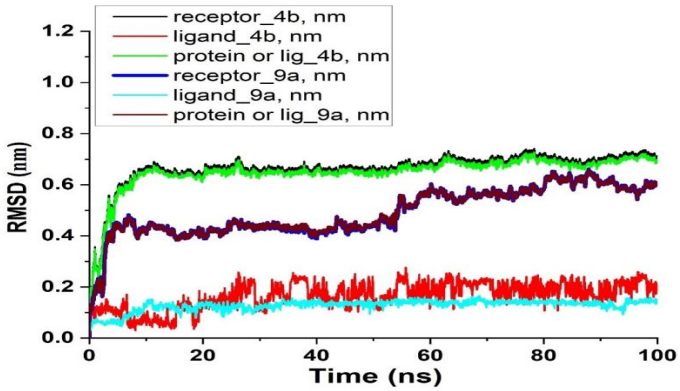

Figure 11: The root mean square deviation (RMSD) of solvated ligand, receptor and protein complex **(TKD: 1M17)**during 100 ns MD simulation time.

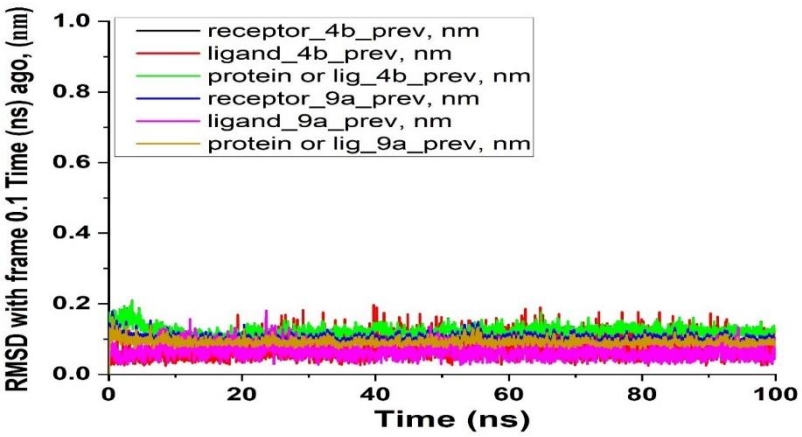

Figure 12. The root mean square deviation (RMSD) vs frame reference 0.1 ns ago of solvated ligand, receptor and protein complex **(TKD: 1M17)** during100 ns MD simulation time.

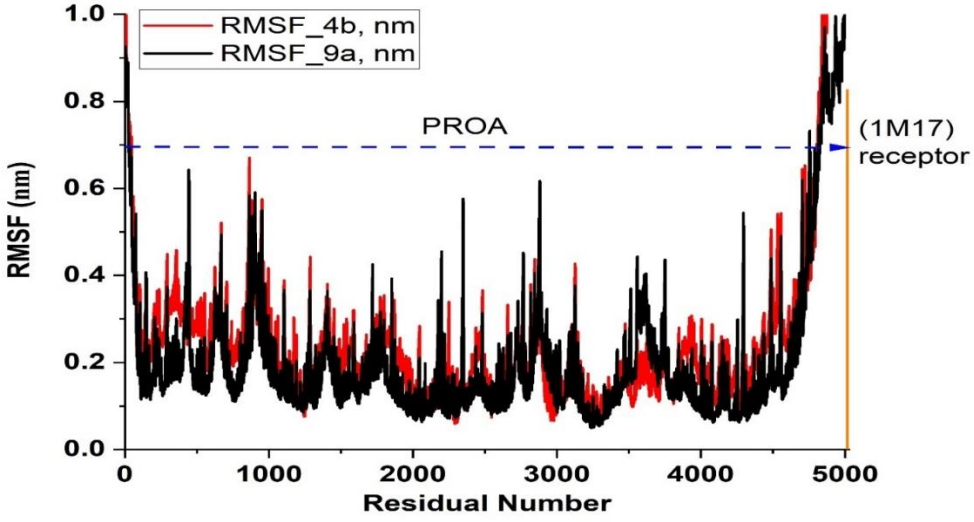

Figure 13. The root mean square fluctuation (RMSF) of solvated ligand, receptor and protein complex **(TKD: 1M17)** during 100 ns MD simulation time.

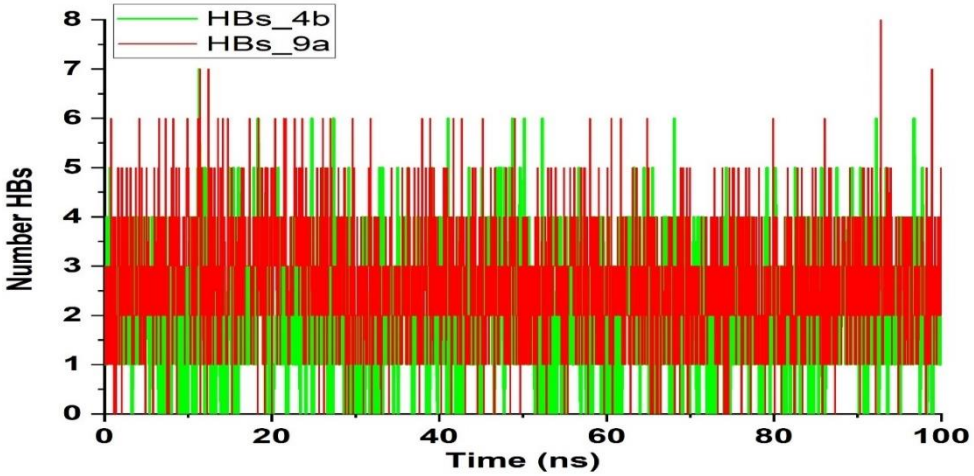

Figure 14: Number of average hydrogen bonding interaction between proteins receptor and Ligand in solvated protein complex **(TKD: 1M17)** during 100 ns MD simulation time.

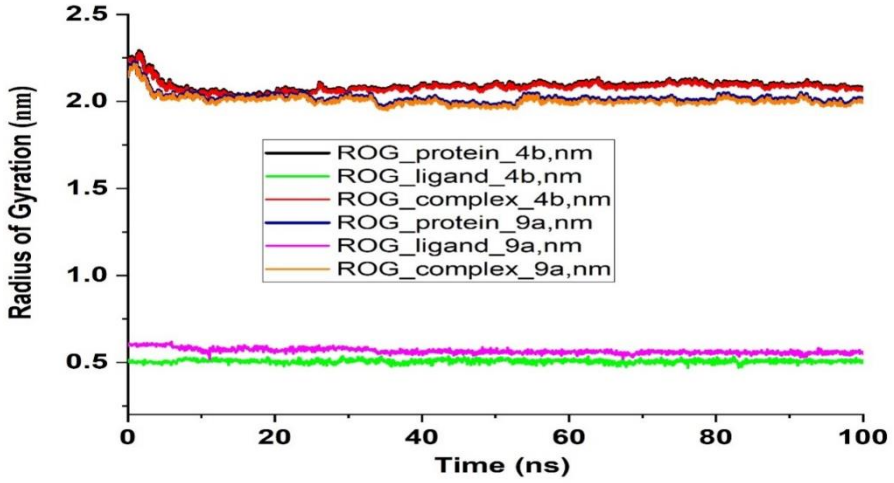

Figure 15.Radius of gyration (Rg) of solvated ligand, receptor and protein complex **(TKD: 1M17)** during 100 ns MD simulation time.

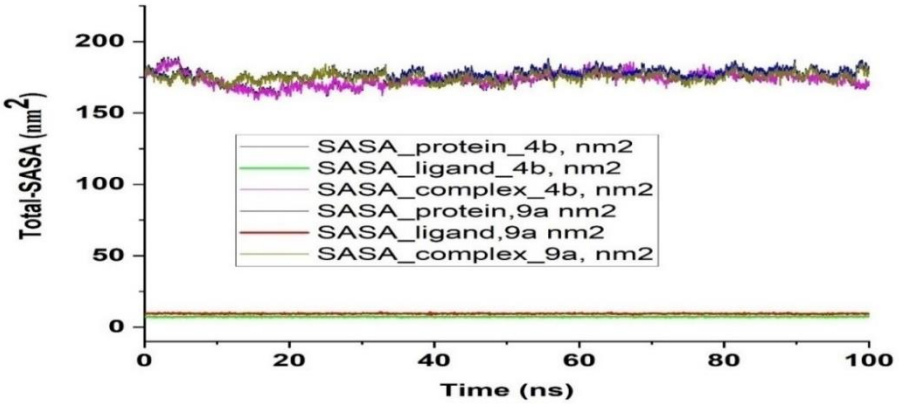

Figure 16: Solvent accessible surface area (SASA) analysis for solvated ligand, receptor, and protein complex **(TKD: 1M17)** during 100 ns MD simulation time.

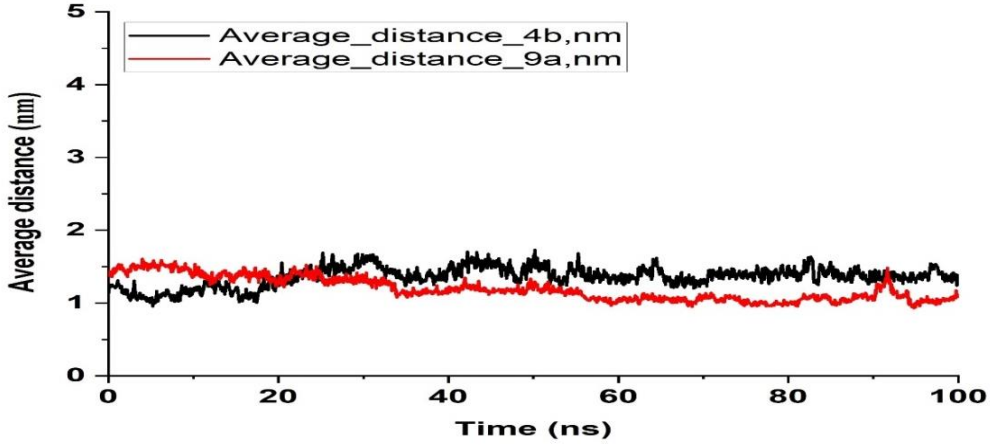

Figure 17: Average distance between the ligand center vs center of mass analysis of solvated protein complex **(TKD: 1M17)** during 100 ns MD simulation time.

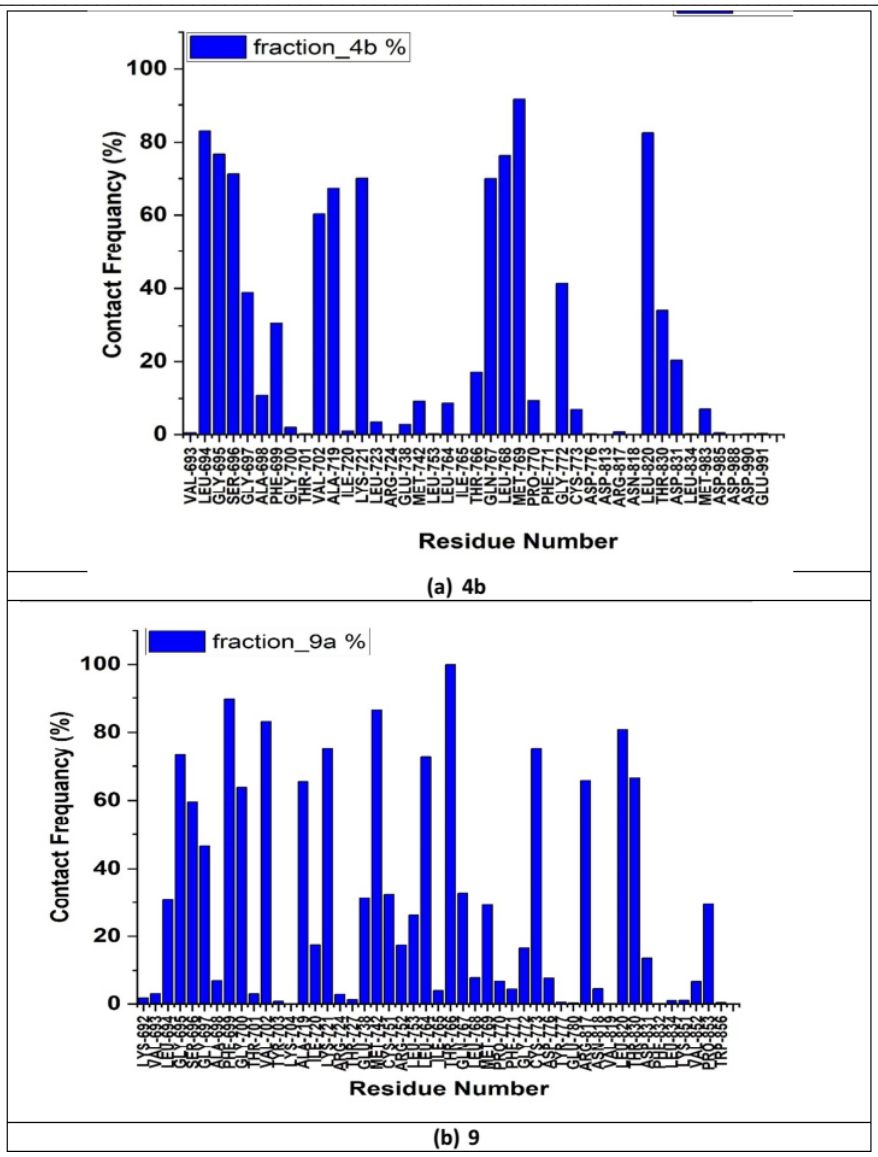

Figure 18: Contact frequency percentage analysis for protein–ligand complexes **(TKD: 1M17)** during 100 ns MD simulation time

3.3. Binding free energies

A popular method for accurately determining the binding free energies of receptor-vaccine complexes is the molecular mechanics energy technique (MM/GBSA and PBSA). GBSA combines the generalized Born and surface area continuum solvation model, while the one-average molecular mechanics Poisson–Boltzmann surface area (MM-PBSA) approach [57,78–80] is path-independent and calculates the free energy of binding by analyzing ensembles of the initial and final states. MM-PBSA is more efficient than MM-GBSA. Both techniques are considered reliable, less computationally demanding, and more productive than docking scores [64,77,81]. The binding free energy of the simulated complexes was calculated based on molecular dynamics (MD) simulation results to validate protein affinity predictions from docking studies for receptor-ligand complexes. Snapshots taken from system trajectories (100 ns) were analyzed using the gmx_MMPBSA tool based on AMBER tools MMPBSA.py with GROMACS files [57]. The computed energy contributions for MM-GBSA and MM-PBSA for both **1M17-4b** and **1M17-9** complexes are summarized in Table 11. High negative values indicate strong interactions and high receptor-ligand affinity, while positive net binding energy indicates reduced docking stability. The net binding free energy of the **1M17-4b** complex was calculated as −22.88 or −15.96 kcal/mol for GBSA and PBSA, respectively. For the **1M17-9** complex, the values were −33.46 or −21.89 kcal/mol, respectively. Analysis of individual energy components revealed that van der Waals and electrostatic energy contributions were significant in binding affinity and supported complex formation. Specifically, van der Waals energy and electrostatic energy values were −33.34 (−54.03) and −31.93 (−14.42 kcal/mol) for **1M17-4b** and **1M17-9** complexes, respectively. Surface and non-polar component energies showed moderate contributions, with values of −4.28 (−7.1) and −6.15 (−5.81 kcal/mol) for **1M17-4b** and **1M17-9** complexes, respectively. The net binding free energy follows the order of **1M17-9**<**1M17-4b**, indicating that the **1M17-9** complex forms a more stable receptor-ligand affinity complex than **1M17-4b**, with differences of 10.58 (5.93 kcal/mol) for GBSA and PBSA, respectively.

These findings suggest that the **1M17-9** complex has a higher binding affinity and is better suited for inhibiting the Epidermal Growth Factor Receptor tyrosine kinase domain. This correlates strongly with the experimentally observed biological effectiveness of the designed drug construct.

Table 11: Summary of the binding Free energy MM/PBSA and MM/GBSA calculated for top docking binding scores of newly synthesized of Coumarin derivatives compounds **(2,3-4a,4b,8 and 9)** with tyrosine kinase domain (**PDB ID: 1M17**) receptor during 100 ns simulation time.

Protein-Ligand complex	ΔE_{VDW}	ΔE_{ELE}	ΔG_{GAS}	MM-GBSA				MM-PBSA			
				ΔE_{GB}	ΔE_{SURF}	ΔG_{SOL}	ΔG_{Bin}	ΔE_{PB}	ΔE_{NPolar}	ΔG_{SOL}	ΔG_{Bin}
1M17- 4b	-33.34	-31.93	-65.26	46.66	-4.28	42.38	**-22.88**	43.36	-6.15	49.3	**-15.96**
1M17- 9	-54.03	-14.42	-68.44	42.08	-7.1	34.98	**-33.46**	52.36	-5.81	46.56	**-21.89**

ΔE_{VDW} = van der Waals energy; ΔE_{ELE} = electrostatic energy;ΔG_{GAS} = gas phase free energy;ΔG_{sol} = solvation free energy;ΔE_{SURF} = Surface energy;ΔE_{GB} = generalized Born energy;ΔE_{PB} = Poisson–Boltzmann energy;ΔE_{NPolar} = non-polar energy**;** ΔG_{bin} = calculated total binding free energy (kcal/mol)
MM-GBSA= molecular mechanics generalized Born surface area; MM-PBSA= Molecular mechanics Poisson–Boltzmann surface area.

Physicochemical and pharmacokinetics profile of the most active compounds and ADME screening

ADME screening was performed with Lipinski Rule of Five[24], for the most active comounds using a freely accessible web-server at supercomputing facility for bioinformatics and computational biology, This rule predicts the various properties of the drugs such as, molecular mass, lipophilicity, total number of hydrogen bond donor, total number of hydrogen bond acceptors and molar refractivity Table: 12

Table (12): Molecular properties of the molecules under study. (A) Pharmacokinetics and Medicinal chemistry (B) Physicochemical properties

Compound	(A) Pharmacokinetics and Medicinal chemistry		
	3	**4(b)**	**9**
Gastrointestinal absorption	high	Low	Low
Blood–brain barrier permeation	No	No	No
Cytochrome P450 1A2 inhibitor	Yes	No	Yes
Cytochrome P450 2D6 inhibitor	Yes	No	No
Cytochrome P450 3A4 inhibitor	Yes	Yes	No
Druglikeness (Lipinski rule)	Yes	Yes	No 2 violations MW>500 NorO>10
Pains	0 alerts	0 alerts	0 alerts
leadlikness	Yes	No 1 violation MW>350	No 3 violations MW>350 Rotors >7 Xlogp3>3.5
Bioavailability score	0.55	0.55	0.17

Compound	(B)Physicochemical properties		
	3	**4(b)**	**9**
Molecular formula	**$C_{16}H_{12}N_2O_4S$**	**$C_{24}H_{22}N_4O_5S$**	**$C_{23}H_{27}N_5O_7S_2$**
Molecular weight (g/mol)	328.3441	478.5218	657.7196
Lipophilicity (LogP)	2.9071	1.9697	3.35
RO5 Violations	0	0	3
RO3 Violationa	4	5	5
Rotable bond	5	5	9
H-Bonds acceptor atoms	6	6	9
H-bonds donor atoms	1	4	3
Molar refractivity	87.72	137.49	182.83
Polar surface area (Consensus)TPS	117.51	154.42	200.0
Num.of heavy atoms	23	34	46
Num. of arom.heavy atoms	15	12	27
Water solubility	Moderately soluble	Poorly soluble	insoluble

Physical therapy and treatment the negative effects experienced by cancer patients

The novel science of rehabilitation body engineering (hand therapy) employs the soft tissue areas and their components as an alternative approach to treating a wide range of diseases, complementing other conventional treatment methods. Additionally, it has proven effective in addressing certain conditions [82-84] that are resistant to traditional medical approaches. This is achieved by applying specific pressure techniques to soft tissue areas to improve the functioning of body organs.

Artificial intelligence (AI) is also increasingly utilized in various modules of hand rehabilitation robots. AI integration not only expands the capabilities of these robotic systems but also enhances their precision, effectiveness, and intelligence. This advancement reduces the strain on medical resources while improving patient comfort and engagement during rehabilitation [85]. In particular, AI contributes significantly to human-robot collaboration in assisted training modes for hand rehabilitation. While rehabilitation robots offer numerous advantages, they also come with limitations [85]. These technologies support the mental and intellectual aspects of therapy, emphasizing that treatment should begin and conclude with a holistic approach. This approach incorporates complementary and preventive strategies that minimize reliance on chemical drugs and invasive surgeries.

Rehabilitative methods have transformed the lives of many individuals, enabling them to live free of pain and discomfort without resorting to life-threatening or ineffective procedures. The body engineering techniques [82-84]developed by Dr. Alboqai who focued on activating the body and mitigating the adverse effects experienced by cancer patients through the following:Treating neuromuscular tension, activating the muscular system, and rehabilitating motor-related side effects in cancer patients.These methods incorporate body engineering, manual therapy, and therapeutic exercises to restore affected organs to their pre-disease functionality. This is to say, body engineering reactivates and restores the functionality of weakened or impaired body systems caused by various factors, offering a non-invasive and effective solution through the science of rehabilitation [82-84].

References

[1] B.B.Shaik; N.K. Katari, ; P.Seboletswe; R. Gundla;N.D.Kushwaha; V.Kumar; P. Singh; R. Karpoormath ; M.D.Bala, Recent Literature Review on Coumarin Hybrids as Potential Anticancer Agents Anti-Cancer Agents in Medicinal Chemistry (Formerly Current Medicinal Chemistry - Anti-Cancer Agents), Volume 23, Number 2, 2023, pp. 142-163(22)

[2] F. N. Takla, W. A. Bayoumi, S. M. El-Messery & M. N. A. Nasr Developing multitargetcoumarin based anti-breast cancer agents: synthesis and molecular modelingstudyScientific Reports volume 13, (2023) Article number: 13370 (2023)

[3] K. B. Patel [a] , S. Mukherjee [b] , H. Bhatt [c] , D.Rajani [d] , I. Ahmad [ef] , H. Patel [f] , P.Kumari Synthesis, docking, and biological investigations of new coumarin-piperazine hybrids as potential antibacterial and anticancer agents Journal of Molecular Structure 1276 (2023) 134755

[4] J. Stamos, M.X. Sliwkowski, C. Eigenbrot, Structure of the epidermal growth factor receptor kinase domain alone and in complex with a 4-anilinoquinazoline inhibitor, J. Biol. Chem. 277 (2002) 46265–46272.

[5] V.M.M.Pérez R,C.Cortés;I.C. López-Santillán,.; A.Salas-Casas, Inflammation in Cancer Development Mexican Journal of Medical Research ICSA, 2022, vol. 10, no. 19, 48-51

[6] X. Wang,[1,2,3] M.E. Reyes,[1,2,3] D. Zhang,[1,2,3] Y.Funakoshi,[1,2,3] A. P. Trape,[1,2,3] Y. Gong,[1,4] T. Kogawa,[1,2,3] B. L. Eckhardt,[1,2,3] H. Masuda,[1,2,3] D. A. Pirman, Jr,[5] ,P. Yang,[6] J.M. Reuben,[1,7] W. A. Woodward,[1,8] C. Bartholomeusz,[1,2,3] G. N. Hortobagyi,[3] D.Tripathy,[3] and N. T. Ueno[1,2,3] EGFR signaling promotes inflammation and cancer stem-like activity in inflammatory breast cancer Oncotarget. 2017 Sep 15; 8(40): 67904 67917. doi: 10.18632/oncotarget.18958PMCID: PMC5620223 PMID: 28978083

[7] S. H. Emam, R. A. Hassan, E. O. Osman, M. I. A. Hamed, A.M. Abdou, M. M. Kandil; E. Ma. Elbaz; D. S. Mikhail; Coumarin derivatives with potential anticancer and antibacterial activity: Design, synthesis, VEGFR-2 and DNA gyrase inhibition, and in silico studies Drug development research:13February 2023 https://doi.org/10.1002/ddr.22037

[8] A.Álvarez-Mercado[1,2,3],A.C.Casals[4], C.Alfonso[4],J.C.Reyes[5] , M. Carnero[4] ,A.S.Gonzalez[6],A.C.Ramírez [5,6] ,J.Sancho [7,8] and C.Peralta[4],* InsightsintoGrowthFactorsin Liver Carcinogenesis and Regeneration :An Ongoing Debateon Minimizing Cancer Recurrence after Liver Resection Biomedicines 2021,9,1158. https: //doi.org/ 10.3390/ biomedicines 9091158

[9] M. L. Uribe; I,Marrocco, and Y,Yarden; EGFR in Cancer: Signaling Mechanisms, Drugs, and Acquired ResistanceCancers (Basel). 2021 Jun; 13(11): 2748. doi: 10.3390/cancers13112748 PMID: 34206026

[10] T. Zubair[1] and D. Bandyopadhyay[1,2] Small Molecule EGFR Inhibitors as Anti-Cancer Agents: Discovery, Mechanisms of Action, and Opportunities Int J Mol Sci. 2023 Feb; 24(3): 2651 doi: 10.3390/ijms24032651 PMCID: PMC9916655 PMID: 36768973

[11] F.F. Alblewi [1];M. H. Alsehli [1]; Z. M. Hritani [1], A.Eskandrani [1], W. H. Alsaedi [1], M.O. Alawad [2], A. A Elhenawy [3 4], H. Y. Ahmed [5], M. S. A El-Gaby [3], T. H. Afifi [1], R. M. Okasha [1] Synthesis and Characterization of a New Class of Chromene-Azo Sulfonamide Hybrids as Promising Anticancer Candidates with the Exploration of Their EGFR, h CAII, and MMP-2 Inhibitors Based on Molecular Docking Assays Int J MolSci 2023 Nov 24;24(23):16716. doi: 10.3390/ijms242316716.

[12]T. Zubair, and D. Bandyopadhyay Small Molecule EGFR Inhibitors as Anti-Cancer Agents: Discovery, Mechanisms of Action, and Opportunities Int. J. Mol. Sci. 2023, 24(3), 2651; https://doi.org/10.3390/ijms24032651

[13] Q. Pan, Y. Lu, L. Xie, D. Wu , R. Liu*, W. Gao, K. Luo , B. He And Y. Pu* Recent Advances in Boosting EGFR Tyrosine Kinase Inhibitors-Based Cancer Therapy Cite this: Mol. Pharmaceutics 2023, 20, 2, 829–852Publication Date:January 1, 2023

[14] E.ChunHei Ho, R.Qiu, E. Miller, M.T.Bilotta, D. F.Gerald, A. Antignani**;** Antibody drug conjugates, targeting cancer-expressed EGFR, exhibit potent and specific antitumor activity Biomedicine & Pharmacotherapy, January 2023, 11404 https://doi.org/10.1016/j.biopha.2022.114047

[15] S. Rao ,B. Thibault, L. Peyrard , A.L. L. Lombard , M. Rupp ,C. Thauvin and B. J. Jean-Claude Quantitative Analysis of the Potency of Equimolar Two-Drug Combinations and Combi-Molecules Involving Kinase Inhibitors In Vitro: The Concept of Balanced Targeting Int. J. Mol. Sci. 2021, 22(17), 9569; https://doi.org/10.3390/ijms22179569

[16] Y. Tanaka, T. Ito, Y. Kaku-Ito, K. Tanegashima, G. Tsuji, M. Kido-Nakahara, Y. Oda & T. Nakahara Human epidermal growth factor receptor 3 serves as a novel therapeutic target for acral melanoma Cell Death Discovery volume 9, Article number: 54 (2023)

[17] I.Wang , A. Zeng , M. Zhu , L. Song; Dual inhibition of EGFR-VEGF: An effective approach to the treatment of advanced non-small cell lung cancer with EGFR mutation (Review) International journal of oncology January 3, 2023 https://doi.org/10.3892/ijo.2023.5474

[18] S.Ruth: Toxicity and resistance of tyrosine kinase inhibitor drugs – Evaluation of novel substrates for tyrosine kinases Master's degree program in General Toxicology The University of Eastern Finland, School of Pharmacy June 2023

[19]B.C.Cho [1], A.Simi [2], J.Sabari [3], S.Vijayaraghavan [4], S.Moores [4], A.Spira [5]Amivantamab, an Epidermal Growth Factor Receptor (EGFR) and Mesenchymal-epithelial Transition Factor (MET) Bispecific Antibody, Designed to Enable Multiple Mechanisms of Action and Broad Clinical ApplicationsClinical Lung CancerVolume 24, Issue 2, March 2023, Pages 89-97

[20] R. R. Jr Properties of FDA-approved small molecule protein kinase inhibitorsPharmacologicalResearchVolume 187, January 2023, 106552

[21] P. Y. Lee, Y.Yeoh, T. Y. LowA recent update on small-molecule kinase inhibitors for targeted cancer therapy and their therapeutic insights from mass spectrometry-based proteomic analysis The FEBS journal 21 March 2022**https://doi.org/10.1111/febs.16442**

[22]M.J. Frisch, G.W. Trucks, H.B. Schlegel, G.E. Scuseria, M.A. Robb, J.R. Cheeseman, G. Scalmani, V. Barone, G.A. Petersson, H. Nakatsuji, X. Li, M. Caricato, A. V Marenich, J. Bloino, B.G. Janesko, R. Gomperts, B. Mennucci, H.P. Hratchian, J. V Ortiz, A.F. Izmaylov, J.L. Sonnenberg, D. Williams-Young, F. Ding, F. Lipparini, F. Egidi, J. Goings, B. Peng, A. Petrone, T. Henderson, D. Ranasinghe, V.G. Zakrzewski, J. Gao, N. Rega, G. Zheng, W. Liang, M. Hada, M. Ehara, K. Toyota, R. Fukuda, J. Hasegawa, M. Ishida, T. Nakajima, Y. Honda, O. Kitao, H. Nakai, T. Vreven, K. Throssell, J.A. Montgomery Jr., J.E. Peralta, F. Ogliaro, M.J. Bearpark, J.J. Heyd, E.N. Brothers, K.N. Kudin, V.N. Staroverov, T.A. Keith, R. Kobayashi, J. Normand, K. Raghavachari, A.P. Rendell, J.C. Burant, S.S. Iyengar, J. Tomasi, M. Cossi, J.M. Millam, M. Klene, C. Adamo, R. Cammi, J.W. Ochterski, R.L. Martin, K. Morokuma, O. Farkas, J.B. Foresman, D.J. Fox, Gaussian 09, Revis. C. 01, (2010).

[23]**A.D. Becke,** Density-functional exchange-energy approximation with correct asymptotic behavior, Phys. Rev. A 38 (1988) 3098.

[24]**A.D. Becke,** Density-functional thermochemistry. III. The role of exact exchange, J. Chem. Phys. 98 (1993) 5648–5652.

[25]**B.G. Johnson, M.J. Frisch,** Analytic second derivatives of the gradient-corrected density functional energy. Effect of quadrature weight derivatives, Chem. Phys. Lett. 216 (1993) 133–140.

[26]**C. Lee, W. Yang, R.G. Parr,** Development of the Colle-Salvetti correlation-energy formula into a functional of the electron density, Phys. Rev. B 37 (1988) 785.

[27]**A.D. McLean, G.S. Chandler,** Contracted Gaussian basis sets for molecular calculations. I. Second row atoms, Z= 11--18, J. Chem. Phys. 72 (1980) 5639–5648.

[28]**S.E. Ulic, C.O. Della Vedova, A. Hermann, H.-G. Mack, H. Oberhammer,** Preparation and Properties of Trifluorothioacetic Acid-S-(trifluoromethyl) ester, CF 3C (O) SCF 3, J. Phys. Chem. A 112 (2008) 6211–6216.

[29]**A.E. Reed, F. Weinhold,** Natural bond orbital analysis of near-Hartree--Fock water dimer, J. Chem. Phys. 78 (1983) 4066–4073.

[30]**P. Geerlings, F. De Proft, W. Langenaeker**, Conceptual density functional theory, Chem. Rev. 103 (2003) 1793–1874.

[31]**P.K. Chattaraj, D.R. Roy,** Update 1 of: electrophilicity index, Chem. Rev. 107 (2007) PR46--PR74.

[32]**R.G. Parr, W. Yang,** Density functional approach to the frontier-electron theory of chemical reactivity, J. Am. Chem. Soc. 106 (1984) 4049–4050.

[33]R.G. Parr, R.G. Pearson, Absolute hardness: companion parameter to absolute electronegativity, J. Am. Chem. Soc. 105 (1983) 7512–7516.

[34]P.K. Chattaraj, S. Giri, Stability, reactivity, and aromaticity of compounds of a multivalent superatom, J. Phys. Chem. A 111 (2007) 11116–11121.

[35]R.R. Contreras, P. Fuentealba, M. Galvan, P. Perez, A direct evaluation of regional Fukui functions in molecules, Chem. Phys. Lett. 304 (1999) 405–413.

[36]C. Morell, A. Grand, A. Toro-Labbe, New dual descriptor for chemical reactivity, J. Phys. Chem. A 109 (2005) 205–212.

[37]T. Lu, F. Chen, Multiwfn: a multifunctional wavefunction analyzer, J. Comput. Chem. 33 (2012) 580–592.

[38]W. Humphrey, A. Dalke, K. Schulten, VMD: visual molecular dynamics, J. Mol. Graph. 14 (1996) 33–38.

[39]R. Dennington, T. Keith, J. Millam, GaussView, version 5, Semichem Inc. Shawnee Mission. KS (2009).

[40]G.A. Andrienko, Chemcraf program, https://www.chemcraftprog.com, (2018). https://www.chemcraftprog.com.

[41]M. Froimowitz, HyperChem: a software package for computational chemistry and molecular modeling., version 8.0.7,

Biotechniques 14 (1993) 1010. http://www.hyperchem.com.
[42] **M.E. Elshakre, M.A. Noamaan, H. Moustafa, H. Butt,** Density functional theory, chemical reactivity, pharmacological potential and molecular docking of dihydrothiouracil-indenopyridopyrimidines with human-DNA topoisomerase II, Int. J. Mol. Sci. 21 (2020) 1253.
[43] **D.S. Biovia, others,** Discovery studio modeling environment, (2017).
[44] **H.J.C. Berendsen, D. van der Spoel, R. van Drunen,** GROMACS: A message-passing parallel molecular dynamics implementation, Comput. Phys. Commun. 91 (1995) 43–56.
[45] **S. Páll, M.J. Abraham, C. Kutzner, B. Hess, E. Lindahl,** Tackling exascale software challenges in molecular dynamics simulations with GROMACS, in: Solving Softw. Challenges Exascale Int. Conf. Exascale Appl. Software, EASC 2014, Stock. Sweden, April 2-3, 2014, Revis. Sel. Pap. 2, 2015: pp. 3–27.
[46] **M.J. Abraham, T. Murtola, R. Schulz, S. Páll, J.C. Smith, B. Hess, E. Lindahl,** GROMACS: High performance molecular simulations through multi-level parallelism from laptops to supercomputers, SoftwareX 1 (2015) 19–25.
[47] **R.B. Best, X. Zhu, J. Shim, P.E.M. Lopes, J. Mittal, M. Feig, A.D. MacKerell Jr,** Optimization of the additive CHARMM all-atom protein force field targeting improved sampling of the backbone $φ$, $ψ$ and side-chain $χ$1 and $χ$2 dihedral angles, J. Chem. Theory Comput. 8 (2012) 3257–3273.
[48] **J. Lee, X. Cheng, J.M. Swails, M.S. Yeom, P.K. Eastman, J.A. Lemkul, S. Wei, J. Buckner, J.C. Jeong, Y. Qi, others,** CHARMM-GUI input generator for NAMD, GROMACS, AMBER, OpenMM, and CHARMM/OpenMM simulations using the CHARMM36 additive force field, J. Chem. Theory Comput. 12 (2016) 405–413.
[**49**] **S. Kim, J. Lee, S. Jo, C.L. Brooks III, H.S. Lee, W. Im,** CHARMM-GUI ligand reader and modeler for CHARMM force field generation of small molecules, (2017).
[50] **S. Jo, T. Kim, V.G. Iyer, W. Im,** CHARMM-GUI: a web-based graphical user interface for CHARMM, J. Comput. Chem. 29 (2008) 1859–1865.
[51] **B.R. Brooks, C.L. Brooks III, A.D. Mackerell Jr, L. Nilsson, R.J. Petrella, B. Roux, Y. Won, G. Archontis, C. Bartels, S. Boresch, others,** CHARMM: the biomolecular simulation program, J. Comput. Chem. 30 (2009) 1545–1614.
[52] **S. Nosé, M.L. Klein,** Constant pressure molecular dynamics for molecular systems, Mol. Phys. 50 (1983) 1055–1076.
[53] **S. Nosé,** A molecular dynamics method for simulations in the canonical ensemble, Mol. Phys. 52 (1984) 255–268.
[54] **G.S. Grest, K. Kremer,** Molecular dynamics simulation for polymers in the presence of a heat bath, Phys. Rev. A 33 (1986) 3628.
[55] **T. Darden, D. York, L. Pedersen,** Particle mesh Ewald: An N· log (N) method for Ewald sums in large systems, J. Chem. Phys. 98 (1993) 10089–10092.
[56] **U. Essmann, L. Perera, M.L. Berkowitz, T. Darden, H. Lee, L.G. Pedersen,** A smooth particle mesh Ewald method, J. Chem. Phys. 103 (1995) 8577–8593.
[57] **M.S. Valdés-Tresanco, M.E. Valdés-Tresanco, P.A. Valiente, E. Moreno,** gmx_MMPBSA: a new tool to perform end-state free energy calculations with GROMACS, J. Chem. Theory Comput. 17 (2021) 6281–6291.
58 - Molecular Operating Environment. MOE 2014. 0901.
[59] **M.N.Guptaa[,1], V.N. Uversky;** Biological importance of arginine**:** A comprehensive review of the roles in structure, disorder, and functionality of peptides and proteins International Journal of Biological Macromolecules https://doi.org/10.1016/j.ijbiomac.2023.128646 Received 7 November 2023; Received in revised form 2 December 2023; Accepted 4 December 2023
[60] **N. Guex, M.C. Peitsch**, SWISS-MODEL and the Swiss-Pdb Viewer: an environment for comparative protein modeling, Electrophoresis 18 (1997) 2714–2723.
[61] **R.G. Parr, W. Yang,** Density-Functional Theory of Atoms and Molecules, vol. 16 of International series of monographs on chemistry, (1989).
[62] **M. Defranceschi, C. Le Bris,** Mathematical models and methods for ab initio quantum chemistry, Springer Science & Business Media, 2012.
[63] **L.H. Mendoza-Huizar, C.H. Rios-Reyes,** Chemical reactivity of atrazine employing the Fukui function, J. Mex. Chem. Soc. 55 (2011) 142–147.
[64] **A.H. Hasan, F.A. Abdulrahman, A.J. Obaidullah, H.F. Alotaibi, M.M. Alanazi, M.A. Noamaan, S. Murugesan, S.I. Amran, A.R. Bhat, J. Jamalis, H. Arai, Y. Higashigaki, M. Gotoh, S.Y.S. Yano,** Discovery of Novel Coumarin-Schiff Base Hybrids as Potential Acetylcholinesterase Inhibitors: Design, Synthesis, Enzyme Inhibition, and Computational Studies, Pharmaceuticals 16 (2023) 5755.
[65] **S.A. Khan, K. Rizwan, S. Shahid, M.A. Noamaan, T. Rasheed, H. Amjad,** Synthesis, DFT, computational exploration of chemical reactivity, molecular docking studies of novel formazan metal complexes and their biological applications, Appl. Organomet. Chem. 34 (2020) e5444.
[66] **R.G. Pearson,** Absolute electronegativity and hardness correlated with molecular orbital theory, Proc. Natl. Acad. Sci. 83 (1986) 8440–8441.
[67] **A.K. Chandra, T. Uchimara,** NLO and NBO analysis of Sarcosine-maleic acid by using HF and B3LYP calculations, J. Phys. Chem. A 105 (2001) 3578–3582.
[68] **R. Parthasarathi, J. Padmanabhan, M. Elango, V. Subramanian, P.K. Chattaraj,** Intermolecular reactivity through the generalized philicity concept, Chem. Phys. Lett. 394 (2004) 225–230.
[69] **C. Lee, W. Yang, R.G. Parr,** Local softness and chemical reactivity in the molecules CO, SCN- and H2CO, J. Mol. Struct. Theochem 163 (1988) 305–313.
[70] **G. Naray-Szabo, G.G. Ferenczy,** Molecular electrostatics, Chem. Rev. 95 (1995) 829–847.
[71] **J.S. Murray, P. Politzer,** The electrostatic potential: an overview, Wiley Interdiscip. Rev. Comput. Mol. Sci. 1 (2011) 153–163.

[72]F.J. Luque, J.M. Lopez, M. Orozco, Perspective on "Electrostatic interactions of a solute with a continuum. A direct utilization of ab initio molecular potentials for the prevision of solvent effects," Theor. Chem. Acc. 103 (2000) 343–345.

[73]S. Mirzaei, F. Eisvand, F. Hadizadeh, F. Mosaffa, A. Ghasemi, R. Ghodsi, Design, synthesis and biological evaluation of novel 5, 6, 7-trimethoxy-N-aryl-2-styrylquinolin-4-amines as potential anticancer agents and tubulin polymerization inhibitors, Bioorg. Chem. 98 (2020) 103711.

[74]J.N. Miller, Coumarin-6-sulphonyl chloride: a novel label in fluorimetry and phosphorimetry Part 1. Synthesis and Luminescence Properties, Anal. Chim. Acta 227 (1989) 145–153.

[75]A. Sabt, M. Abdelraof, M.F. Hamissa, M.A. Noamaan, Antibacterial Activity of Quinoline-Based Derivatives against Methicillin-Resistant Staphylococcus aureus and Pseudomonas aeruginosa: Design, Synthesis, DFT and Molecular Dynamic Simulations, Chem. \& Biodivers. 20 (2023) e202300804.

[76]A. Bogoyavlenskiy, I. Zaitseva, P. Alexyuk, M. Alexyuk, E. Omirtaeva, A. Manakbayeva, Y. Moldakhanov, E. Anarkulova, A. Imangazy, V. Berezin, others, Naturally Occurring Isorhamnetin Glycosides as Potential Agents Against Influenza Viruses: Antiviral and Molecular Docking Studies, ACS Omega 8 (2023) 48499–48514.

[77]T.A. Majrashi, A. Sabt, H. Almahli, M.A. El Hassab, M.A. Noamaan, E.B. Elkaeed, M.F. Hamissa, A.N. Maslamani, M.A. Shaldam, W.M. Eldehna, DFT and molecular simulation validation of the binding activity of PDE$δ$ inhibitors for repression of oncogenic k-Ras, PLoS One 19 (2024) e0300035.

[78]R. Kumari, R. Kumar, O.S.D.D. Consortium, A. Lynn, g_mmpbsa A GROMACS tool for high-throughput MM-PBSA calculations, J. Chem. Inf. Model. 54 (2014) 1951–1962.

[79]N.A. Baker, D. Sept, S. Joseph, M.J. Holst, J.A. McCammon, Electrostatics of nanosystems: application to microtubules and the ribosome, Proc. Natl. Acad. Sci. 98 (2001) 10037–10041.

[80]S. Pronk, S. Páll, R. Schulz, P. Larsson, P. Bjelkmar, R. Apostolov, M.R. Shirts, J.C. Smith, P.M. Kasson, D. Van Der Spoel, others, GROMACS 4.5: a high-throughput and highly parallel open source molecular simulation toolkit, Bioinformatics 29 (2013) 845–854.

[81]K.E. Machaba, N.N. Mhlongo, M.E.S. Soliman, Induced mutation proves a potential target for TB therapy: a molecular dynamics study on LprG, Cell Biochem. Biophys. 76 (2018) 345–356.

[82]M. K. Alboqai and T. M. A Eldebss. Advanced Therapeutic Technology in Hand Therapy: A Side-Effect-Free Approach to Soft Tissue Rehabilitation Through Body Engineering. Glob. Jor. Sc. Res. (2024) in press

[83]Mohamed. K. Alboqai and Taha. M. A Eldebss , Novel Trend in Therapeutic Technology via Hand Therapy Through Body Engineering Approach to Soft Tissue Rehabilitation; LAMBERT Academic Publishing (2024)ISBN: 978-620-8-11949-2

[84]Alboqai, M. K Introduction to rehabilitation engineering for manual therapy sciences. National Library Department.. (2017). ISBN: 978-9957-67-209-6. Deposit Number: 6256/12/2017

[85]Gonzalez, A., Garcia, L., Kilby, J. et al. Robotic devices for paediatric rehabilitation: a review of design features. BioMed Eng OnLine 20, 89 (2021). https://doi.org/10.1186/s12938-021-00920-5